12 Metal Radionuclides for Molecular Imaging

The doubter is a true man of science; he doubts only himself and his interpretations, but he believes in science.

Claude Bernard

12.1 Introduction

Several prominent investigators have recently stated that the future of nuclear medicine is molecular imaging and theranostics [1, 2]. Nuclear medicine now provides diagnostic, prognostic, predictive, and intermediate endpoint biomarkers in oncology, cardiology, neurology, and infectious and inflammatory disorders. Whole-body target expression can be quantified and used for predicting therapy response. Treatment-induced metabolic changes serve as early prognosticators of therapy effectiveness. At the same time, technologic advances such as total-body hybrid PET/CT PET/MR imaging are revolutionizing the diagnostic capabilities of PET systems. In the last 20 years, ^{18}F-labeled PET tracers dominated the field of molecular imaging. As of January 2022, there are 16 FDA-approved PET tracers, out of which 10 are based on ^{18}F and only 4 or based on radiometals (Table 12.1) [3]. With the FDA approval of ^{68}Ga-Dotatate, ^{68}Ga-Dotatoc, ^{68}Ga-PSMA−11, and ^{64}Cu-dotatate, the future of molecular imaging in the coming decade may be based on PET radiopharmaceuticals with radiometals.

Extensive knowledge, experience, and understanding of the metal chemistry at the tracer level

Table 12.1 Approved metal-based radiopharmaceuticals in clinical use for PET and SPECT

Radiopharmaceutical	Trade name	Decay	Target	Indication	FDA approval
^{111}In-DTPA-octreotide	OctreoScan	*EC*	Somatostatin type II receptor (SSTR-II)	Neuroendocrine tumors	1994
^{99m}Tc-Apcitide (^{99m}Tc-P280)	AcuTect	*IT*	GP II_b/III_a receptor	Deep vein thrombosis (DVT)	1997
^{68}Ga-DOTA-TOC (^{68}Ga-endotreotide)	Somakit	β^+	Somatostatin type II receptor (SSTR-II)	Neuroendocrine tumors	2016, 2019
^{99m}Tc-Hynic-octreotide	Tektreotyd	*IT*			2018
^{68}Ga-DOTATATE	NetSpot®	β^+			2018
^{64}Cu-Dotatate	DetectNet	β^+, β^-, *EC*			2020
^{68}Ga-PSMA-11		β^+	Prostate specific membrane antigen (PSMA)	Prostate cancer	2020

S. Vallabhajosula, *Molecular Imaging and Targeted Therapy*,
https://doi.org/10.1007/978-3-031-23205-3_12

would enable us to develop a number of new molecular imaging radiotracers based on β^+-emitting radiometals. ^{99m}Tc and ^{111}In labeled SPECT radiopharmaceuticals will continue to play a prominent role in the development of SPECT radiopharmaceuticals. Since targeted radionuclide therapy (TRT) is primarily based on metal radionuclides (such as ^{90}Y, ^{177}Lu, ^{225}Ac, and ^{227}Th), the theranostics and personalized medicine dictate that the development of radiopharmaceuticals for imaging and therapy must be based on theranostic pair of radiometals. The advantages of metal-labeled molecular imaging radiotracers can be summarized as follows:

- Easy availability: ^{68}Ga generators are available for easy in-house preparation based on kit production.
- Cyclotron production of metallic nuclides (^{68}Ga, ^{89}Zr, and ^{44}Sc) has been optimized using medical cyclotrons using primarily (*p*,*n*) nuclear reactions.
- Fifty-year experience with the development of bifunctional chelating agents (BFCs) and metal-labeled radiopharmaceuticals.
- Ability to label target specific biomolecules (peptides and proteins).
- Availability of theranostic radionuclide pairs for imaging and therapy.
- High SA of radiometal.
- High SA of metal-labeled peptide and/or protein.
- High in vivo stability of metal-labeled tracers.
- Favorable radiation dosimetry, especially with ^{68}Ga and ^{44}Sc.

12.2 Radiometals for PET and SPECT

Radioisotopes of various metals useful for PET and SPECT imaging studies are listed in Tables 12.2 and 12.3. The selection of a radiometal for

Table 12.2 Important radioisotopes of metals useful for PET and SPECT

Metal		Stable isotopes		Radioactive isotopes				
Z	Name	Nuclide	%	Nuclide	$T_{½}$ (h)	Decay	% β^+ emission	SA (Ci μmole^{-1})
21	Scandium	^{45}Sc	100	^{44}Sc	3.927	EC, β^+	β^+ (94.27)	
22	Titanium	^{46}Sc	8.25	^{45}Ti	3.10	EC, β^+	β^+ (84.82)	
		^{47}Sc	7.44					
		^{48}Sc	73.72					
		^{49}Sc	5.41					
		^{50}Sc	5.18					
27	Cobalt	^{59}Co	100	^{55}Co	17.53	EC, β^+	β^+ (77)	
29	Copper	^{63}Cu	69.17	^{60}Cu	0.39	EC, β^+	β^+ (93)	
		^{65}Cu	30.83	^{61}Cu	3.32	EC, β^+	β^+ (62)	
				^{62}Cu	0.163	EC β^+	β^+ (98)	19,310
				^{64}Cu	12.80	EC, β^+, β^-	β^+ (19)	245
31	Gallium	^{69}Ga	60.10	^{66}Ga	9.45	EC, β^+	β^+ (62)	331
		^{71}Ga	30.90	^{67}Ga	78.24	EC, γ		40
				^{68}Ga	1.14	EC, β^+	β^+ (90)	2766
37	Rubidium	^{85}Rb	72.16	^{82}Rb	75 s	EC, β^+	β^+ (96)	
		^{87}Rb	27.84					
39	Yttrium	^{89}Y	100	^{86}Y	14.74	EC, β^+	β^+ (34)	213
40	Zirconium	^{90}Zr	51.45	^{89}Zr	78.48	EC, β^+	β^+ (23)	39.9
		^{91}Zr	11.22					
		^{92}Zr	17.15					
		^{94}Zr	17.38					
		^{96}Zr	2.80					
49	Indium	^{113}In	4.3	^{110}In	1.1	EC, β^+, γ	β^+ (71)	
		^{115}In	95.7	^{111}In	67.2	EC, γ		47
	Technetium	No stable isotope		^{94m}Tc	0.88	EC, β^+	β^+ (72)	
				^{99m}Tc	6.01	IT		522

Table 12.3 The most common nuclear reactions for the production of positron-emitting radiometals

Radiometal	Nuclear reaction	Target abundance (%)	Proton energy range (MeV)
^{44}Sc	^{44}Ca (*p*,*n*) ^{44}Sc	2.086	~11
^{45}Ti	^{45}Sc (p,n) ^{45}Ti	100	~11
^{61}Cu	^{61}Ni (*p*,*n*) ^{61}Cu	1.25	9–12
^{64}Cu	^{64}Ni (*p*,*n*) ^{64}Cu	0.91	8–15
^{66}Ga	^{66}Zn (*p*,*n*) ^{66}Ga	27.8	8–15
^{67}Ga	^{68}Zn (*p*,2*n*) ^{67}Ga	19.0	12–22
^{68}Ga	^{68}Zn (p,n) ^{68}Ga	>97%	11–12
^{86}Y	^{86}Sr (*p*,*n*) ^{86}Y	9.86	10–15
^{89}Zr	^{89}Y (*p*,*n*) ^{89}Zr	100	~14
^{94m}Tc	^{94}Mo (*p*,*n*) ^{94m}Tc	9.12	10–15
^{110}In	^{110}Cd (*p*,*n*) ^{110}In	12.5	10–20
^{111}In	^{112}Cd (*p*,2*n*)^{111}In	24.0	12–22

labeling a specific peptide or protein is dependent on several factors, such as physical half-life, SA, type(s) of decay and emission(s), energy of the emission(s), and cost and availability. In addition, pharmacokinetics, drug delivery of the radio-metal-complex to the target site and clearance of the radiometal complex from both the target and nontarget tissues are all important factors that determine the selection of an appropriate radiometal in tracer development.

Among the β⁺-emitting metallic nuclides, ^{64}Cu (T = 12.6 h), ^{66}Ga ($T_{½}$ = 9.45 h), ^{86}Y ($T_{½}$ = 14.74 h), and ^{89}Zr ($T_{½}$ = 3.27 days) are more appropriate for development of commercial PET radiopharmaceuticals since they can be transported across the country. For most of these metallic radionuclides, cyclotron production methods have been optimized, using medical cyclotrons using primarily (*p*,*n*) nuclear reactions (Table 12.3). The two nuclides with short half-lives, ^{68}Ga ($T_{½}$ = 68.3 min) and ^{62}Cu ($T_{½}$ = 9.76 min) can be produced on demand from commercial generator systems without the need for an on-site cyclotron. However, cyclotron production methods for ^{68}Ga have been well optimized both for liquid targets (3–5 GBq) and solid targets (50–100 GBq). Also, the ^{82}Sr($T_{½}$ = 25 days) → ^{82}Rb ($T_{½}$ = 75 seconds) generator (cardioGen-82®) has been FDA approved for myocardial perfusion studies. The positron-emitting metals such as ^{44}Sc, ^{45}Ti, and radiometals ^{55}Co have optimal half-lives and positron kinetic energies and are actively investigated by several groups for labeling small molecules, and peptides for molecular imaging studies.

12.2.1 Specific Activity of Radiometals

The SA of the radiometal is an indicator of potency; the higher the SA of the radiometal, the higher is the SA of the radiometal-labeled biomolecule. The theoretical SA of carrier-free radiometals, useful for developing PET and SPECT radiotracers, is shown in Table 12.2. The practical SA that can be achieved by cyclotron production or by generator, however, depends on many other factors. In general, SA of all β⁺-emitting radiometals is much higher than the corresponding SPECT nuclides, except for ^{89}Zr. Also, the SA of ^{68}Ga (2.766 Ci nmol^{-1}) is even much higher than that of ^{18}F (1.71 Ci nmol^{-1}).

The maximum theoretical SA of ^{64}Cu is ~4000 mCi μg^{-1} but, the cyclotron production of ^{64}Cu achieves a maximum SA of ~200 mCi μg^{-1} at EOB [4]. In practice, purity control difficulties in solid target production often cause much lower SA to be delivered due to cold Cu contamination. In comparison, the SA of generator-produced ^{62}Cu is >70,000 mCi μg^{-1} and levels approaching this maximum can be routinely achieved.

12.2.2 Decay Characteristics of Radiometals

The intensity of β⁺ emission from a radionuclide or branching ratio directly affects the rate of true coincidences because lower β⁺ decay fraction results in fewer annihilation events per MBq [5].

Also, the β^+ must slow down and rest before it can annihilate with an electron. Thus, annihilation takes place in a spherical volume whose radius depends on the energy. Consequently, with PET, positrons with lower energy will have shorter range in tissue and higher expected spatial resolution [6]. In addition, the ability to visualize a lesion depends on the amount of activity in the lesion compared to the background. The short half-life metals such as ^{68}Ga are ideal for radiotracers, such as peptides and small molecules, which clear from circulation rapidly.

Another important consideration is the emission of γ photons associated with certain positron emitters. The number of photons, amount of energy, and the abundance (%) for several radiometals useful for PET are shown in Table 12.4. Except for ^{62}Cu, ^{64}Cu, and ^{68}Ga, all other radiometals have significant gamma emissions. Radionuclides, such as ^{66}Ga, ^{86}Y, ^{89}Zr, and ^{124}I, have a very high proportion of γ emission compared to the intensity of β^+ emission. Detection of gamma photons or scattered photons, along with annihilation photons, may reduce the coincidence count rate performance (true counts) in several different ways [7, 8]. Also, the associated gamma emission will have a significant impact on the radiation dose to the patient, radiation exposure, and burden to the technical staff [5].

For the development of PET tracers, it is important to recognize that each radionuclide has unique imaging characteristics with respect to image quality, biological vector compatibility, cost, availability, and dosimetry. In principle, PET performance, in terms of spatial resolution and the range in tissue (Table 12.5), will change with positron-emitting radionuclide due to the kinetic energy of the positron [6, 9, 10]. Therefore, it is vital to understand and characterize the variables that will impact image quality. Among the radiometals listed in Tables 12.4 and 12.5, the positron from ^{64}Cu has lowest energy compared to that from ^{86}Y and ^{66}Ga. In contrast, the positron from ^{89}Zr has energy comparable to that of ^{18}F. As a result, ^{89}Zr has become more popular for the molecular imaging studies, especially with monoclonal antibodies.

Table 12.5 Range of positrons in water[a]

Radionuclide	T½	β + Emean (KeV)	CDSA range[b] (mm)
^{72}As	26 h	1170	5.16
^{68}Ga	68 m	830	3.37
^{86}Y	14.7 h	660	2.50
^{89}Zr	78.4 h	396	1.23
^{18}F	110 m	250	0.62
^{52}Mn	5.59 d	242	0.59

[a]Data from [6]
[b]Continuous slowing down approximation (CSDA) for the average energy of positron

Table 12.4 Positron-emitting radionuclides and decay characteristics

	T½	β^+ decay	β^+ Energy (MeV)		Major γ energy (KeV) and abundance (%)		
Nuclide		(%)	E_{max}	E_{mean}	1	2	3
^{44}Sc	3.927	94.27	1.473	0.632	1157 (100)		
^{45}Ti	3.10	84.82	1.027	0.439			
^{55}Co	17.53	76.0	1.498	0.573	931 (75)	1408 (16.9)	
^{62}Cu	0.163	97.83	2.937	1.319			
^{64}Cu	12.80	17.6	0.653	0.2782	1346 (0.47)		
^{66}Ga	9.49	57.0	4.153	1.75	1039 (37)	2751 (23)	4.295 (4)
^{68}Ga	1.14	88.9	1.899	0.830	1077 (3)		
^{82}Rb	75 s	95.4	3.382	1.481	777 (13.4		
^{86}Y	14.74	31.9	3.141	0.662	443 (17)	627 (33)	1.076 (83)
^{89}Zr	78.48	22.74	0.902	0.396	908 (100)		
^{94m}Tc	0.88	72.0	2.47	1.0942	871 (94.2)	1522 (4.5)	1869 (5.7)

12.3 Chemistry of Radiometals

Some of the important physical properties and the electron configuration of various metals useful in developing molecular imaging probes are summarized in Table 12.6. Among these metals, gallium and indium are post-transition metals (group 13 or IIIB in the periodic table). All other metals, useful for developing radiopharmaceuticals for molecular imaging, are transition metals with complex coordination chemistries. The therapeutic radionuclides ^{177}Lu (lanthanide), ^{225}Ac, and ^{227}Th (actinides) are included here to compare the chemistry with PET/SPECT nuclides. All the metals in Table 12.6 requite a bifunctional chelating agent (BFC) to complex the radiometal and to form a covalent bond with the targeting vehicle (or vector), such as small molecule, peptide, or protein (monoclonal intact antibodies (mAb) or different size fragments derived from antibodies). Figure 12.1 shows a schematic of metal-based molecular imaging radiopharmaceutical composed of four different components: targeting vehicle, spacer, linker, and chelating agent.

12.3.1 Chelators for Metal Complexation

Coordination chemistry is the study of compounds that have a central metal atom (coordination center) surrounded by molecules or anions, known as ligands. The ligands are attached to the central metal atom by coordinate bonds (also known as dipolar or dative bonds), in which both electrons in the bond are supplied by the same atom on the ligand. The atom within a ligand that is bonded to the central metal atom or ion is called the donor atom. The number of donor atoms attached to the central atom, or ion, is called the coordination number. In coordination compounds, the metal ions have two types of valences; *primary valence* (also known as oxidation state) refers to the ability of metal ion to form ionic bonds with oppositely charged ions, while *secondary valence* (also known as coordination number) refers to the ability of a metal ion to bind to Lewis bases (ligands) to form complex ions. Therefore, the coordination number is the number of bonds formed by the

Table 12.6 Physical and chemical characteristics of radiometals

	Transition metals					Post-transition metals		Lanthanides	Actinides	
Property	Sc	Cu	Y	Zr	Tc	Ga	In	Lu	Ac	Th
Atomic number	21	29	39	40	43	31	49	71	89	90
Group	3	11	3	4	7	13	13	3	n/a	n/a
Block	d	d	d	D	d	p	p	D	f?	f
Atomic radius (pm)	162	128	181	160	136	122	163	174	126	108–135
Ionic radius (pm)	75–87	80	90–108	109	56	47– 62	62–92	86–103	112	105
Electron structure	[Ar] $3d^1$ $4s^2$	[Ar] $3d^{10}$ $4s^1$	[Kr] $4d^1$ $5s^2$	[Kr] $4d^2$ $5s^2$	[Kr] $4d^5$ $5s^2$	[Ar] $3d^{10}$ $4s^2$ $4p^1$	[Kr] $4d^{10}$ $5s^2$ $5p^1$	[Xe] $4f^{14}$ $5d^1$ $6s^2$	[Rn] $6d^1$ $7s^2$	[Rn] $6d^2$ $7s^2$
Electronegativity	1.36	1.90	1.22	1.33	1.90	1.81	1.78	1.27	1.1	1.3
Oxidation state	+3	+1, +2	+3	+4	−1 to +7	+3	+3	**+3**	+3	+4
Coordination number	6–8	4	6–9	6–8	2–8	6	4–8	6–9	9–10	>8

Data for effective ionic radii were derived from http://abulafia.mt.ic.ac.uk/shannon/ptable.php

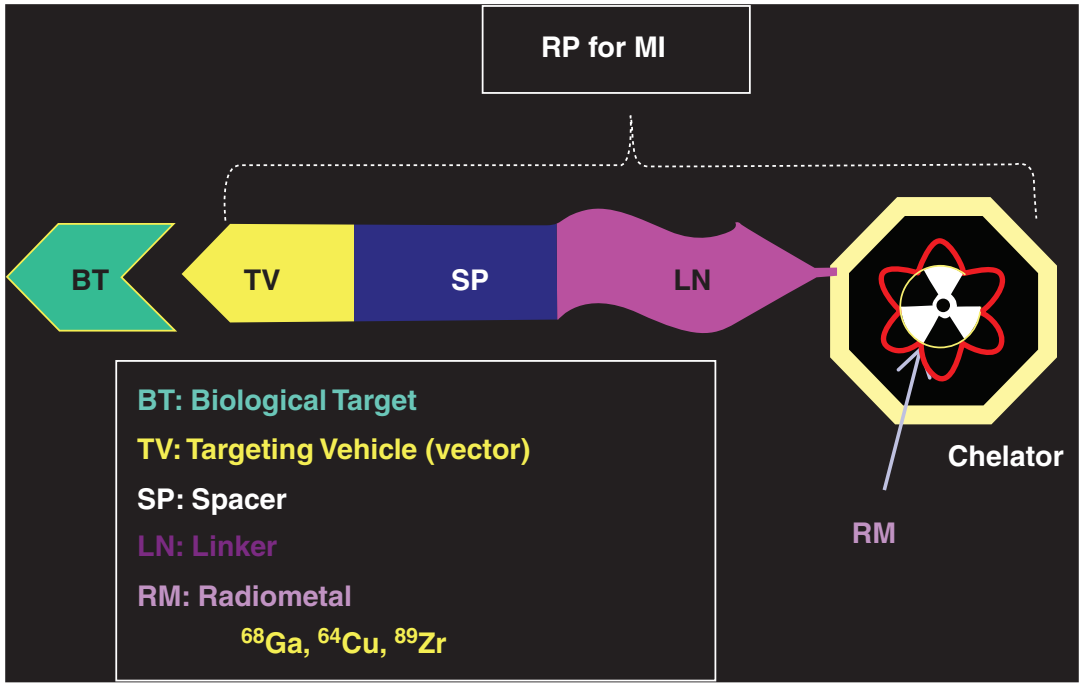

Fig. 12.1 Schematic of a metal-based molecular imaging radiopharmaceutical for PET and SPECT

metal ion with the atoms (that can donate a pair of electrons) in a chelating agent. This number varies from 2 to 8 (Table 12.6), depending on the size, charge, and electron configuration of the metal ion. The ligand geometric arrangements of coordination compounds can be linear, square planar, tetrahedral, or octahedral, depending on the coordination number.

Monodentate ligands (such as F^-, Cl^- ions) donate one pair of electrons to the central metal atoms. Polydentate ligands, also called chelates or chelating agents, donate more than one pair of electrons to the metal atom forming a stronger bond and a more stable complex. The metal complex can be neutral or charged. When the metal complex is charged, it is stabilized by neighboring counter-ions. These metal complexes are called chelate complexes and the formation of such complexes is called chelation or complexation and coordination. Alfred Werner, a Swiss chemist, won the Nobel Prize in chemistry in 1913 for his work on transition metal complexes.

As shown in Fig. 18.1, the radiometals used for imaging and targeted therapy form strong coordinate covalent bonds with chelating agents. The main goal in the synthesis of metal-based radiopharmaceuticals is to form a robust coordination complex that is stable and does not release the free metal in vivo. BFCs serve the dual purpose of radiometal complexation and bioconjugation to the targeting vehicle (or the vector). Two classes of chelators known as acyclic and macrocyclic have been developed in the last four decades for the development of metal-based radiopharmaceuticals.

12.3.1.1 Chelating Agents

Some of the important acyclic and macrocyclic chelators used in the synthesis of metal-based therapeutic radiopharmaceuticals are shown in the Figs. 12.2 and 12.3 and summarized in Table 12.7. Each of these chelating agents differ in size and offer different donor groups such as carboxylic acids, alcohols, amines, thiols, and phosphonic acids. Since the chelating agent must form complexes with the metal ion with high thermodynamic stability and kinetic inertness at pH 5–7.5, chelating agents must meet specific

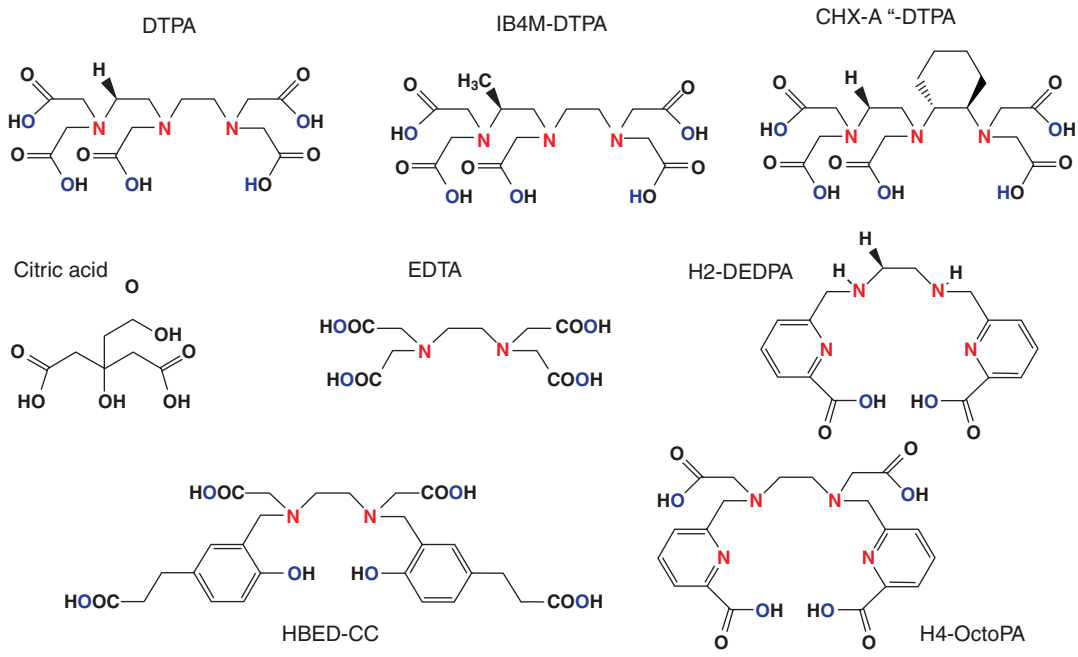

Fig. 12.2 Acyclic chelators used to prepare radiometal therapeutic radiopharmaceuticals. The nitrogen and oxygen donor atoms for metal coordination shown in color

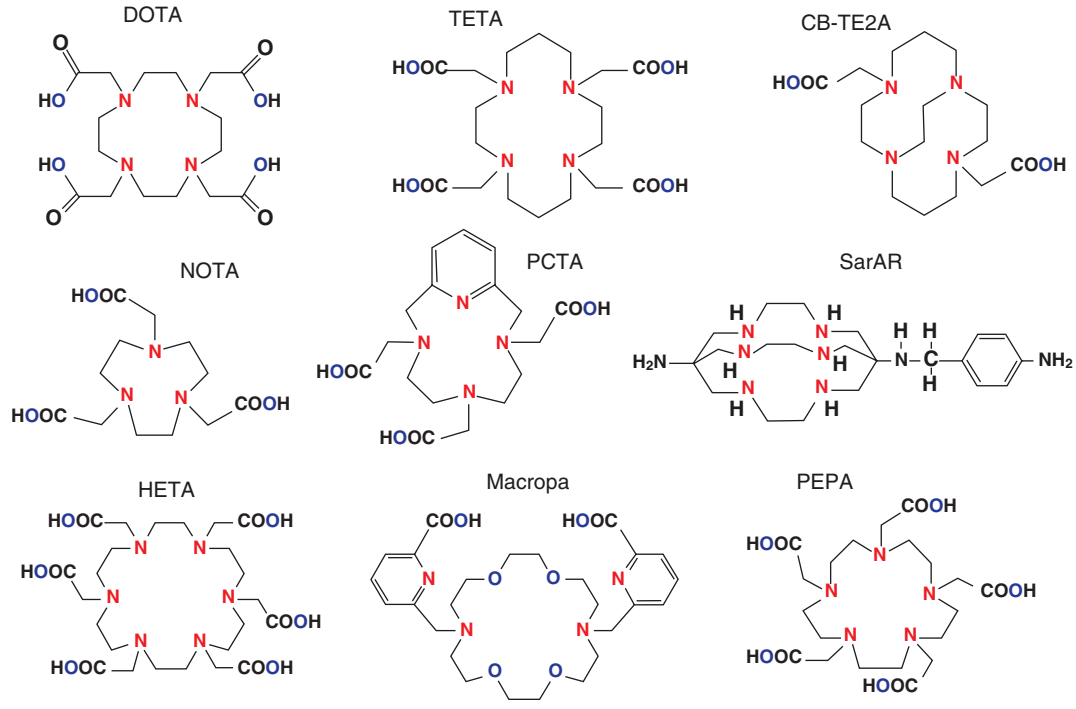

Fig. 12.3 Macrocyclic chelators used to prepare radiometal therapeutic radiopharmaceuticals. The nitrogen and oxygen donor atoms for metal coordination shown in color

Table 12.7 Acyclic and macrocyclic chelators used to prepare radiometal therapeutic radiopharmaceuticals

Chelator	Chemical name	Donor atoms	CN	Metal
DTPA	Diethylenetriaminepentaacetic acid	N_3O_5	8	Ga, In
CHX-A"-DTPA	Trans-(S,S)-cyclohexane-1,2-diamine-pentaacetic acid	N_3O_5	8	Y
EDTA	Ethylenediaminetetraacetic acid	N_2O_4	6	Ga, In
H_2dedpa	1,2-[[6-(carboxy)-pyridin-2-yl]-Methylamino] ethane	N_4O_2		
H_4octopa	N,N′-bis(6-carboxy-2-pyridylmethyl)-Ethylenediamine-N,N′-diacetic acid	N_4O_4	8	
HBED-CC	3-[3-[4-[5-(2-carboxyethyl)-2-hydroxyphenyl]-1,4-bis (carboxymethylamino)butyl]-4-hydroxyphenyl]propanoic acid	N_2O_6	8	Ga
Desferrioxamine B (DFO)	1-Amino-6,17-dihydroxy-7,10,18,21-tetraoxo-27-(N-acetyl hydroxylamino)-6,11,17,22-tetraazaheptaeicosane	O_6	6	Zr
NOTA	1,4,7-triazacyclononane-1,4,7-tri-acetic acid	N_4O_3	6	Ga, Sc
DOTA	1,4,7,10-tetraazacyclododecane-1,4,7,10-tetraacetic acid	N_4O_4	8	In, Sc, Ga, Y, Bi, Lu, Ac, Th
TETA	1,4,8,11-tetraazacyclotetradecane-1,4,8,11-tetraacetic acid	N_4O_4	8	Cu
CB-TE2A	4,11-bis-(carboxymethyl)-1,4,8,11-tetraazabicyclo[6.6.2]-hexadecane	N_4O_2	6	Cu
SarAr	1-*N*-(4-aminobenzyl)-3,6,10,13,16,19-hexaazabicyclo[6.6.6]eicosane-1,8-diamine (SarAr)	N_6	6	Cu
PCTA	3,6,9,15-Tetraazabicyclo[9.3.1]pentadeca-1(15),11,13-triene-3,6,9-triacetic acid	N_4O_3	7	Ga, Cu

requirements. The fundamental metal ion characteristics (Table 12.6), such as atomic number, charge, and radius, which vary from metal ion to metal ion, and result in distinct preferences for geometry, coordination number, and ionic/covalent bond contribution. For optimal stability, the coordinating functional groups of the chelator should adopt the favored geometry of the metal ion while, simultaneously, satisfying metal coordination requirements to prevent competition from extraneous ligands, especially in biological systems [11–13]. The metal-ligand compatibility is dependent on the hard-soft acid-base (HSAB) character of the involved atoms.

Most of the radiometals are hard acids with 2+ and 3+ as their major oxidation states in aqueous solution. Hard metal ions have high charge density, have nonpolarizable electron shells, and tend to form predominantly ionic bonds, in which electrostatic attraction is the primary driving force of bond formation. A useful metric for hard-soft character is the Drago-Wayland parameter, I_A, ($I_A = E_A/C_A$) which conveys the electrostatic (EA) and covalent (CA) contributions to the formation constants of Lewis acid-base complexes (includes metal complexes) in aqueous solution [13]. A higher value of I_A indicates greater hardness of the metal (Table 12.8). Therefore, hard metal ions prefer hard donating groups (e.g., carboxylic acids), which possess dense anionic character (e.g., carboxylic acids). Conversely, soft metals have low charge density and polarizable electron shells, and form covalent bonds with softer, more electron-disperse donor groups.

Acyclic Chelating Agents

Diethylenetriaminepentaacetic acid (DTPA) was one of the first acyclic chelators (Fig. 12.2) used in the 1980s to label peptides and antibodies with ^{111}In and ^{90}Y. DTPA has been successfully used to develop FDA approved peptide, ^{111}In-DTPA-Octreotide (Octreoscan®), a SPECT imaging agent for the detection of neuroendocrine tumors. Subsequently, several DTPA analogs such as

Table 12.8 Metal-chelate complexes and stability parameters[a]

Metal			DOTA			DTPA		
	Hardness	I_A	CN	Log K_{ML}	p*M*	CN	Log K_{ML}	p*M*
Sc^{3+}	Hard	10.49	N_4O_4	27.0–30.8	23.9–26.5	N_3O_5	26.3–27.4	
Cu^{2+}	Borderline soft		N_4O_2	22.7	17.6			
Ga^{3+}	Hard	7.07	N_4O_2	21.3–26.1	15.2	N_3O_4	24.3	20.2
Y^{3+}	Hard	10.64	N_4O_4	24.3–24.9	19.3–19.8	N_3O_5	21.9–22.5	17.6–18.3
In^{3+}	Borderline hard	6.3	N_4O_4	23.9	18.8	N_3O_5	29.0–29.5	24.4–25.7

[a]The table is revised from reference Kostelnik and Orvig 2018

1B4M-DTPA (Tiuxetan) and CHX-A"-DTPA were developed to improve the in vivo stability of radiolabeled complexes. To increase the stability, preorganizing groups have been attached to the carbon backbone which can stabilize the conformation of the free chelator to form a more kinetically stable complex. Tiuxetan was used to develop the FDA-approved ^{111}In or ^{90}Y-labeled anti-B1 mAb (Zevalin®) for the targeted therapy of patients with non-Hodgkin's lymphoma (NHL).

EDTA analogs such as HBED-CC, H4-Octopa were also developed to improve stability of metal-labeled complexes in vivo. HBED-CC chelator was used to prepare FDA approved ^{68}Ga-PSMA-11 for imaging PSMA-positive prostate cancer. Acyclic chelators are of special interest when antibodies or short-lived radiometals are used because radiolabeling can be performed within minutes at room temperature.

Macrocyclic Chelating Agents

Macrocyclic ligands are not only multi-dentate, but because they are covalently constrained to their cyclic form, they allow less conformational freedom. The ligand is said to be pre-organized for binding and there is little entropy penalty for wrapping it around the metal ion. To increase the kinetic stability of metal complexes, the structure of acyclic polyamino-polycarboxylate ligands was modified to cyclic chelates such as DOTA, NOTA, TETA, PEPA, and HEHA (Fig. 12.3).

The first synthesis of DOTA was reported in 1976 by Stetter and Frank. DOTA (also known as H_4DOTA) is derived from the macrocycle, cyclen. Subsequently, macrocyclic BFCs based on DOTA were developed by strategically incorporating functionalized side chain to facilitate binding to antibodies [14]. In the last three decades, DOTA chelator and its derivatives have become the most important chelating agents in the development of both diagnostic and therapeutic radiopharmaceuticals.

DOTA-based chelators tend to exhibit high in vivo stability for most trivalent radiometals but, require somewhat elevated temperatures and/or longer complexation reaction times. For antibodies, higher temperature is not appropriate but, if peptides are used as vector molecules, the slow kinetic of formation can be overcome by heating (close to 100 °C) or the use of microwave technology, which usually does not destroy the biomolecule. Once the metal is inside the macrocyclic tetraaza core, the metal will remain there under physiological conditions [15].

12.3.1.2 Stability of Metal-Chelate Complex

The electronegativity and oxidation state play a major role in the formation of metal-ligand complexes. Evaluation of a chelator's metal affinity requires knowledge of its acid-base properties (protonation constants) and the thermodynamic stability of its metal complexes. The metal ions dissolved in water are complexed to form aqua ions. However, in the presence of a chelating agent or the ligand (L) with greater affinity for the metal than the affinity of OH^- ion for the metal, the formation of metal-chelate complex is preferred, as shown below.

$$M + L ? ML \tag{12.1}$$

$$K_s = \frac{[ML]}{[M][L]} \tag{12.2}$$

In the above equation, [ML] represents the concentration of the metal-ligand complex, while

[M] and [L] represent the concentrations of the free metal and the free ligand, respectively. The stability of the metal-ligand complex is defined by the stability constant ($K_{S\ or}$ K_{ML}) when the system reaches an equilibrium between interacting chemical species [16]. The higher the value of K_{ML}, the greater the thermodynamic stability of the metal-ligand complex (Table 12.8). The values of K_{ML} (such as 10^4 or 10^{30}) are normally represented as log K_{ML} values (such as 4 and 30). A more useful thermodynamic parameter is the *pM value* ($-\log[M]_{Free}$), and the pM values are linearly correlated with K_{ML} values and express the extent to which a metal ion complex is formed in solution under physiologically relevant conditions [13]. The K_{ML} values are usually determined for metal-chelate reactions under ideal conditions of buffer, pH and temperature, and do not necessarily reflect the stability of metal-ligand complex in vivo. For a specific metal, a chelating agent with a higher *pM* value is desirable but, does not predict kinetic stability.

It is important to appreciate that the stability constant can only reveal the direction of the reaction (formation or dissociation) but, not the rate of the reaction. For example, when a purified metal-ligand complex is injected into the circulation, the rate of dissociation of the complex may be significantly increased due to extreme dilution of the complex. Therefore, the *kinetic stability* of the metal-ligand complex is very important under in vivo conditions where competing ions (such as Fe^{3+}, Ca^{2+}, Cu^{2+}, Zn^{2+}) and ligands (serum proteins, enzymes) may augment the transchelation of the radiometal [16]. A quantity known as *conditional stability constant* can be measured or estimated as a function of pH and in the presence of different amounts of other competing ligands. The in vivo stability or the kinetic inertness of a radiotracer is evaluated more appropriately based on biodistribution studies in animal models using a radiometal-labeled chelate conjugated target vehicle (vector) with high radiochemical purity (RCP) and optimal specific activity (SA).

12.3.1.3 Bifunctional Chelating Agents

When a chelating agent has two different functional groups (such as alcohol, carboxylic acid, or amide), it is called a bifunctional chelating agent (BFC or BFCA). The BFC consists of a chelating moiety to complex the radiometal and a functional group for the covalent attachment of the biomolecule (such as peptide and mAb). The BFCs contain a side chain (not participating in the chelation of metal) for conjugation to a peptide or protein. The side chain can be attached to the carbon backbone of the chelate (C-functionalized chelate) or by substitution to one of the nitrogen atoms in the molecule. C-functionalized chelating agents are preferable and provide greater stability to the metal-chelate complex, since all the donor atoms (nitrogen and oxygen) will be available for coordination with the metal ion. Once an appropriate chelating agent is selected for a specific metal, BFC is synthesized by adding the functional group to the chelating agent. Some of the most common commercially available BFCs used in the synthesis of radiometal complexes for therapeutic applications are shown in Fig. 12.4. In the last three decades, an array of reactive functional groups for conjugation of BFCs to proteins have been reported in the literature [13, 17–19].

As shown in Fig. 12.1, in the design of target-specific metal-labeled radiopharmaceuticals, a pharmacokinetic modifying (PKM) linker is attached between the targeting vehicle and the BFC-radiometal complex. The RKM Linkers and spacers are often employed to separate the BFC and the bioconjugate for two reasons. The first is to avoid detrimental interactions of the biomolecule with the coordination complex formation of the chelator with the radiometal. The second more important reason is to modify the excretion kinetics and optimize the biodistribution and pharmacokinetics of the radiolabeled complex to enhance the target/background (T/B) ratios. These linkers can be neutral or charged (cationic or anionic), or metabolically cleavable and biodegradable. A simple hydrocarbon chain will increase lipophilicity while a peptide sequence

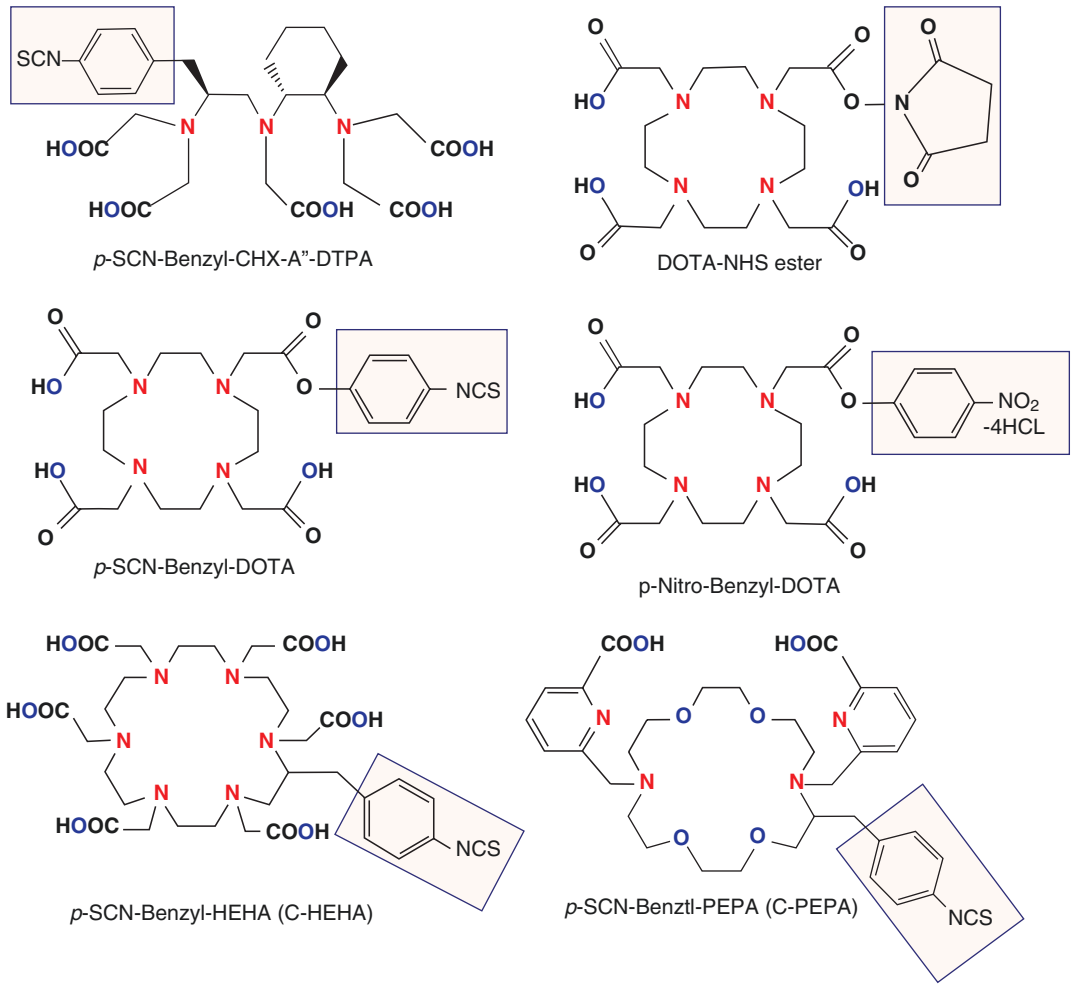

Fig. 12.4 Bifunctional chelating agents (BFCA) commonly used to conjugate a biomolecule and complex a radiometal. The nitrogen and oxygen donor atoms for metal coordination shown in color

will increase hydrophilicity and renal clearance. Polyethylene glycol (PEG) linker can alter the excretion kinetics and improve tumor targeting.

Coupling of BFC to Biomolecule

To combine a biomolecule with a BFC, two different strategies are generally used. In the pre-conjugation strategy, the BFC is first radiolabeled with the metal and the purified radiometal-BFC complex is then conjugated to the biomolecule. Since the conjugation step is not quantitative and requires additional purification steps, pre-conjugation strategy may not be practical for routine use. In the post-conjugation radiolabeling approach, the BFC is first conjugated to the biomolecule and the purified BFC-biomolecule complex (precursor) can be stored under appropriate conditions for several months or years before the labeling with the radiometal is performed. To achieve high labeling yields and radiochemical purity (RCP), the precursor mass (molar ratio) should be significantly more than the radiometal mass. This strategy is more practical and suitable for routine manufacture of therapeutic radiopharmaceuticals.

Coupling of the biomolecule or the targeting vector to the BFC often relies on nucleophilic attack from the bioconjugate. Electrophiles, such

as anhydrides, bromo- or iodoacetamides, isothiocyanates, N-hydroxysuccinimide (NHS) esters, carboxylic acid active esters, and maleimides are typical groups for conjugation that have been developed to modify biomolecules with the appropriate BFCAs. Primary amines are reactive towards isothiocyanates and active esters, while maleimide is reactive towards thiols [19]. The use of copper mediated "click-chemistry" and Diels-Alder coupling has also been utilized in the preparation of radiometal complexes of biomolecules. Some of the most important and routinely used strategies for conjugating BFC to a biomolecule are summarized in Fig. 12.5.

The activation of a carboxylate group of the BFC via an active ester, which reacts with a primary amine of the biomolecule (sidechain of a lysine residue or N-terminal amine of a peptide) leads to a peptide bond that is highly stable under physiological conditions. An example of the activation of the carboxylate is the formation of N-hydroxysuccinimide (NHS) ester. Isothiocyanates are reactive to amines, as well. They may be formed from nitro groups and react in aqueous solutions at pH 9–9.5 with primary amines to form thiourea bonds. This reaction restricts this method to biomolecules that are not sensitive to alkaline conditions. Maleimides react selectively with the thiol groups (from cysteine) in the biomolecules and form a thioether bond with the BFC. The pH for this reaction is close to 7 so that this reaction is ideal for biomolecules. Anhydrides of the BFC react with primary amines of the biomolecules. The dianhydride of DTPA might react with the biomolecule to form a DTPA-monoamide as well as a DTPA-bisamide and cross-linkage of two biomolecules may occur. To avoid cross-linkage, asymmetric anhydrides of DTPA and DOTA have been developed and used.

12.3.2 Chemistry of Post-transition Metals

Both gallium and indium have a filled *d* shell and three electrons in the outermost shell (Table 12.6). For these two metals, the most important oxidation state is +3. Their coordination chemistry is some-

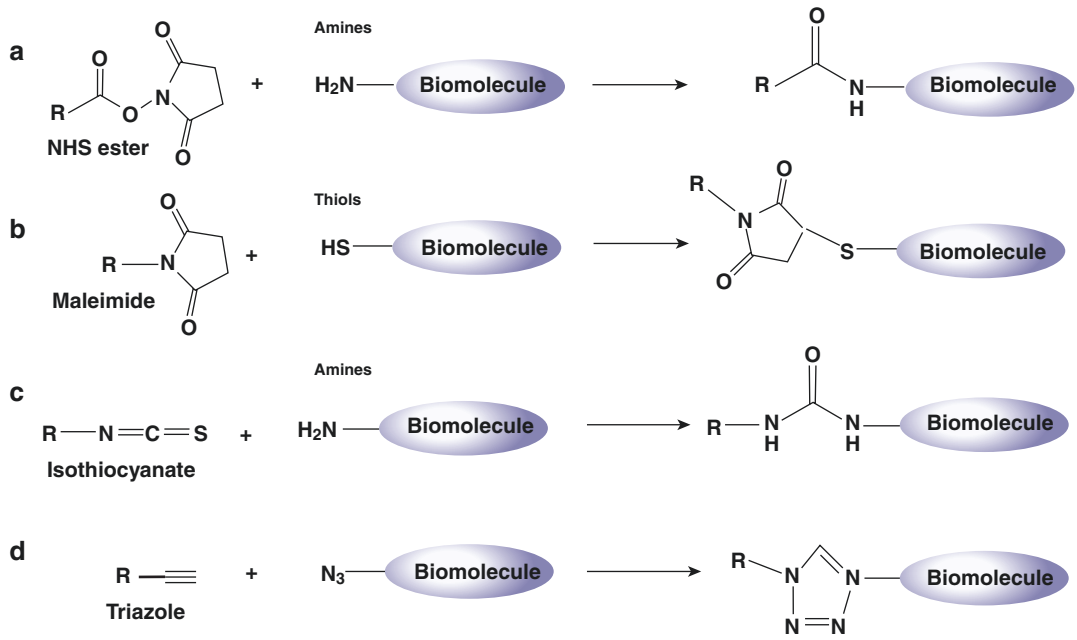

Fig. 12.5 Conjugation reactions commonly used for the covalent attachment of BFCA (R) to a targeting biomolecule with the formation of an amide (**a**), thioether (**b**), thiourea (**c**), and triazole bond (**d**)

what similar; however, due to small differences in their ionic radii and electronegativities, minor but, significant differences do exist in their chemistries. The trivalent metals share chemical characteristics with ferric ion (Fe^{3+}). This similarity with ferric ion is important in the development of radiopharmaceuticals since iron is an essential element in the human body and a number of iron binding proteins, such as transferrin (in blood), exist to transport, and store iron in vivo. As a result, the atoms of iron always compete with these radiometals for specific binding with proteins, such as transferrin, lactoferrin, and ferritin, in vivo [20].

The aqueous chemistry of Ga and In is dominated by their ability to form strong complexes (both soluble and insoluble) with the hydroxyl ion. The fully hydrated (hexaaquo) M^{3+} ions are only stable under acidic conditions. As the pH is raised above 3, these three metals form insoluble hydroxides ($M(OH)_3$). A variety of OH intermediates are formed as a function of pH and the mass of the metal. Gallium is more amphoteric than indium and yttrium. As a result, at physiological pH, gallium exists predominantly as a soluble species, $[Ga(OH)_4]^-$ (gallate) [21]. With indium, soluble $[In(OH)_4]^-$ starts forming only at pH values higher than 7.0. The total solubility of these metals at the physiological pH is very limited; very high SAs of radiometals are needed to keep them soluble in water. However, it is a common practice to add weak chelating agents (such as citrate, acetate, or tartrate ion) to complex the metal and prevent precipitation at the neutral pH. For example, ^{67}Ga is used in the clinic as ^{67}Ga-citrate. Following intravenous administration, ^{67}Ga binds to transferrin in plasma and is transported to tumors and infectious foci as "Ga-transferrin complex" [22].

The coordination chemistry of the metallic radionuclide will determine the geometry and stability of the "metal-chelate complex." Both, Ga and In are classified as hard acids and prefer hard bases [20]. It has been shown that in +3 oxidation state, both Ga and In form thermodynamically stable complexes with either 4, 5, or 6 coordinate ligands, with 6-coordiante being the most stable. The advantage of using the acyclic chelators (DTPA and EDTA) is their extremely fast and high radiolabeling efficiency under mild conditions, and greater thermodynamic stability; however, their kinetic lability often results in the dissociation of the radiometal. The macrocyclic chelates (NOTA, DOTA, and TETA), however, provide greater thermodynamic stability as well as kinetic stability. While Ga and In form greater thermodynamically stable complexes with NOTA, DTPA and EDTA, Y prefers DOTA. The labeling kinetics of DOTA-based BFCs is usually slow and much more dependent on the radiolabeling conditions, including the DOTA-conjugate concentration, pH, reaction temperature, heating time, buffer agent and concentration, and presence of other metallic impurities such as Fe^{3+} and Zn^{2+} [23].

12.3.2.1 ^{68}Ga-Labeled Radiopharmaceuticals

The recent FDA and European agencies approval of ^{68}Ga-labeled molecular imaging agents (^{68}Ga-Dotatate, ^{68}Ga-Dotatoc, and ^{68}Ga-PSMA-11) and the development of ^{68}Ga-PET is a true landmark in molecular imaging that will allow for the use of diverse molecules, and receptor analogues in clinical practice. With the introduction of ^{111}In-DTPA-octreotide (OctreoScan), in the 1990s, metal-based molecular imaging agents introduced a paradigm shift in the development of radiopharmaceuticals. But the inherent superiority of PET imaging is a clear advantage compared to planar and/or SPECT (Fig. 12.6). The ability to use ^{68}Ge/^{68}Ga generator up to a year is cost-effective negating the need for an on-site cyclotron [25–28]. Recent developments in the cyclotron production (5–100 GBq) of ^{68}Ga based on liquid [29] and solid targets [30] will also revolutionize the commercial distribution of ^{68}Ga-labeled radiopharmaceuticals [31].

^{68}Ga Generator

The ^{68}Ga generator was first developed in the 1960s for brain imaging studies [32]. Subsequent generators utilized ^{68}Ge germanate adsorbed on tin dioxide and ^{68}Ga was eluted with HCl [33, 34]. The use of a relatively high concentrations of HCl (1.0 N) presents a problem due to the volatility of $GeCl_4$ and the subsequent spread of airborne, long-lived ^{68}Ge contamination. In addi-

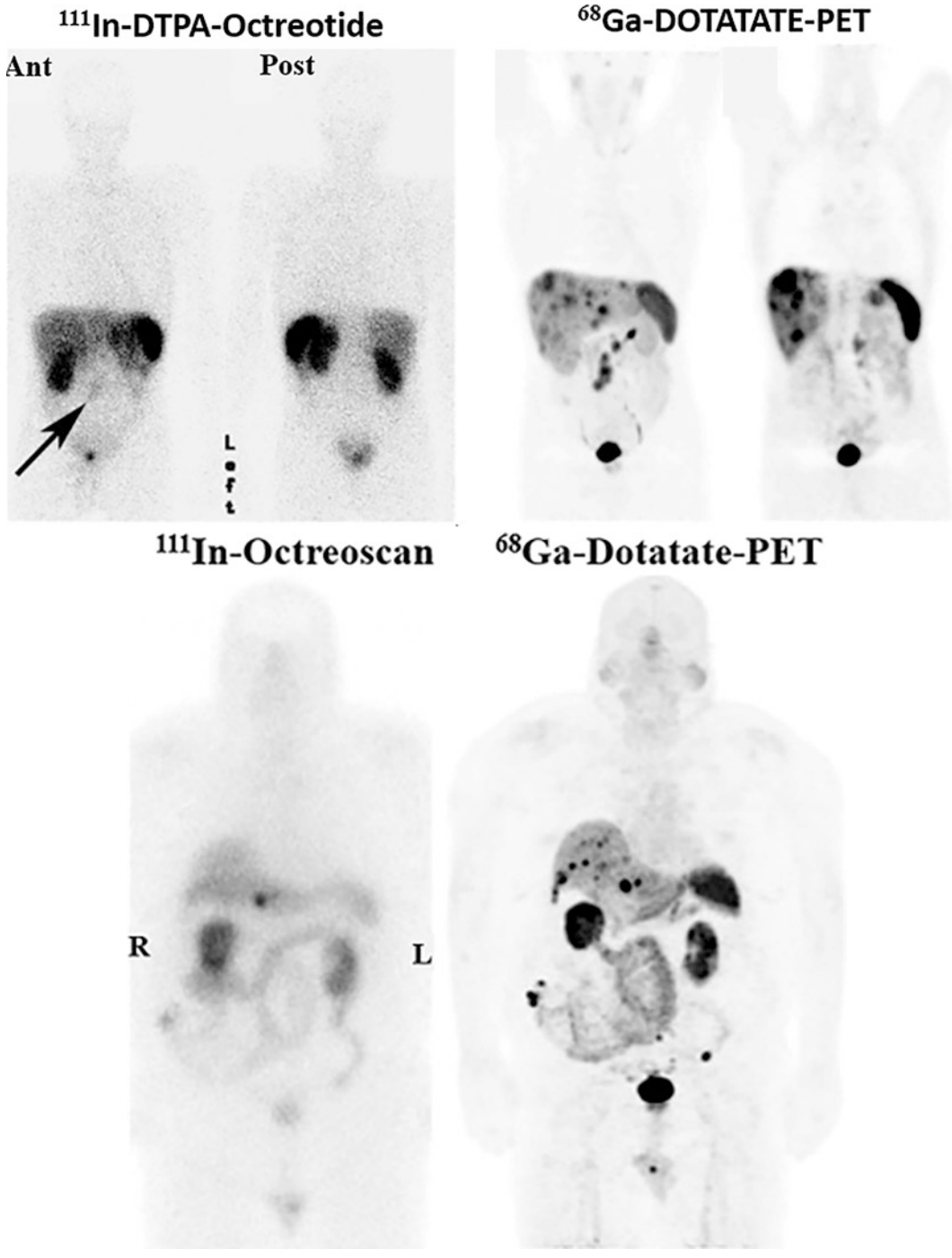

Fig. 12.6 Comparison of ^{68}Ga-Dotatate-PET with ^{111}In-DTPA-octreotide in a patient with low-grade metastatic midgut neuroendocrine tumor (NET). Anterior and posterior whole-body planar ^{111}In-DTPA-octreotide scintigraphy shows low-grade mesenteric metastases but, no liver metastases. ^{68}Ga-DOTATATE PET shows multiple metastases in liver and mesentery [24]

tion, ^{68}Ga is eluted in a large volume of acid (>5 mL), containing metal impurities that are known to bind with high affinity to DOTA. Commercial ^{68}Ga generators (Fig. 12.7) are available based on the use of TiO_2 as an inorganic matrix to immobilize ^{68}Ge in the oxidation state IV^+ [35, 36]. Consequently, ^{68}Ga (III) can be easily separated by eluting it with dilute HCl. It has also been reported that the SA of the generator eluted ^{68}Ga can be as high as 27 Ci μmol^{-1} [37]. Some of these generators, however, are not necessarily optimized for the synthesis of ^{68}Ga-labeled radiopharmaceuticals. The eluates have rather large volumes with a pH of 1, breakthrough of ^{68}Ge (the parent radionuclide) increasing with time or frequency of use, and impurities such as stable Zn(II), Ti(IV), Fe(III). In order to avoid these impurities, additional concentration and purification can be performed using a miniaturized column with organic cation-exchanger resin and hydrochloric acid/acetone eluent [38]. The processed ^{68}Ga fraction can be directly transferred to solutions containing labeling precursors such as DOTATOC. Labeling yields of >95% and specific activities of (50–500 MBq nmol^{-1}) can be obtained under optimized conditions. Further, fully automated synthesis modules (Fig. 12.8) have been developed to prepare ^{68}Ga radiopharmaceuticals for clinical use [39–41].

Fig. 12.7 ^{68}Ge → ^{68}Ga generators from different manufacturers

Fig. 12.8 Examples of automated synthesis modules for the labeling of metal radiopharmaceuticals

^{68}Ga-DOTA-TOC

In the late 1990s, several octreotide analogs conjugated with DOTA chelator were introduced in order to develop ^{90}Y-labeled SST analog for PRRT. Among these SST analogs, DOTATOC was shown to be suitable for labeling with either ^{90}Y or ^{67}Ga [42, 43]. DOTATOC exhibits high affinity (IC_{50}) for human SSTR-2 (14 ± 2.6 nM) with much lower binding affinity for all other human SSTRs. A marked improvement of SSTR-2 affinity was found for Ga-DOTATOC (2.5 nM) compared with the Y-DOTATOC (11 nM) and OctreoScan (22 nM) [44]. In 2001, it was reported that ^{68}Ga-DOTATOC-PET results in high tumor to non-tumor contrast and low kidney accumulation and yields higher detection rates (>30% more lesions) as compared with OctreoScan scintigraphy [45–47]. Since its introduction, ^{68}Ga-DOTATOC has been extensively used in Europe over the last two decades. A systematic review and meta-analysis concluded that ^{68}Ga-DOTATOC is useful for evaluating the presence and extent in disease for staging and restaging, and for assisting in the treatment decision making for patients with NETs [48].

^{68}Ga-DOTA-TOC was approved in several European countries in 2016 (IASOtoc®) and in 2018 (TOCscan®). Also, in Europe a kit preparation for ^{68}Ga-labeling of DOTA-TOC (SomaKit TOC®) was approved by the European Medicines Agency (EMA) in September of 2016. Use of this kit along with an authorized ^{68}Ge/^{68}Ga-generator enables on-site preparation of ^{68}Ga-DOTATOC. In the United States, the FDA approved the ready-to-use ^{68}Ga-DOTATOC in August of 2019. The holder of the NDA (New Drug Application) or marketing authorization is the UIHC–PET Imaging Center (University of Iowa Health Care (UIHC)), in Iowa, USA [49].

^{68}Ga-DOTATATATE

DOTATATE is an SST analog and an SSTR agonist that closely simulates DOTATOC, in which the C-terminal threoninol (an amino alcohol) is replaced by threonine (Fig. 12.9). This chemical modification resulted in a nine-fold higher affinity (1.5 nM) for the SSTR-2 as compared with DOTATOC (14 nM). Also, the affinity of Ga-DOTATATE (0.2 nM) for SSTR-2 is 12 times higher compared to that of Ga-DOTATOC (2.5 nM) [44]. Preclinical studies in animal models demonstrated that DOTATATE may be a better SST analog for the development of radiotracers for imaging and targeted therapy compared to DOTATOC [50, 51]. No human data, however, was available at that time to support the preclinical observations.

Based on direct comparison of PET/CT studies with ^{68}Ga-DOTATOC and ^{68}Ga-DOTATATE it was concluded that both these radiotracers pos-

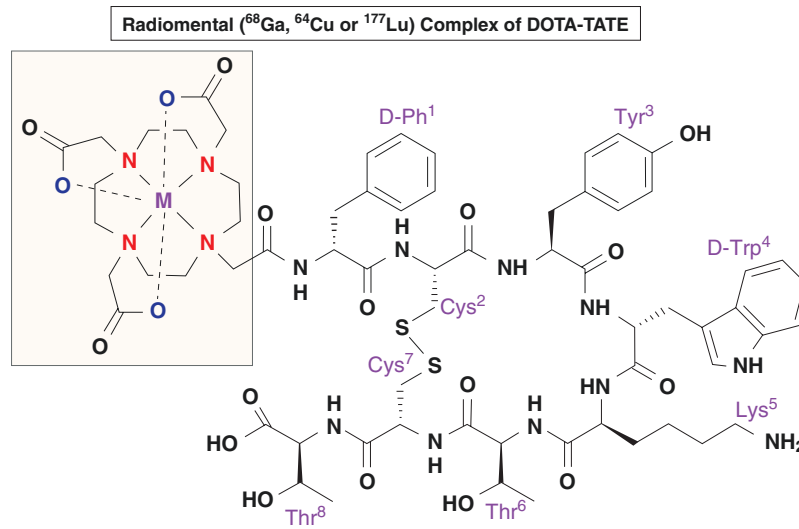

Fig. 12.9 The structure of radiometal- (^{68}Ga, ^{64}Cu, or ^{177}Lu) labeled DOTA-TATE (DOTA-Tyr^3-octreotide) complex

sess a comparable diagnostic accuracy for the detection of NET lesions, with ^{68}GaDOTATOC having a potential advantage. The approximately tenfold higher affinity for the SSTR-2 of ^{68}Ga-DOTATATE does not prove to be clinically relevant. Also, the study found that the SUV_{max} of ^{68}Ga-DOTATOC scans tended to be higher than their ^{68}Ga-DOTATATE counterparts [52].

In June of 2016, the FDA approved ^{68}Ga-DOTATATE (NETSPOT™) for the localization of SSTR positive NETs in adult and pediatric patients. NETSPOT™ is the new market name for Somakit-TATE (a kit for the preparation of ^{68}Ga-dotatate injection using ^{68}Ga chloride from the GalliaPharm ^{68}Ga/^{68}Ga generator from Eckert & Ziegler). ^{68}Ga-dotatate received Orphan Drug Designation from both the FDA and the European Medicines Agency (EMA) in March of 2014.

^{68}Ga-PSMA-HBED-CC (or ^{68}Ga-PSMA-11)

Prostate specific membrane antigen (PSMA) was discovered as a novel antigenic marker in prostate cancer cells. PSMA, is also known as glutamate carboxypeptidase II (GCPII), N-acetyl-L-aspartyl-L-glutamate peptidase I (*NAALADase I*) or N-acetyl-aspartyl-glutamate (*NAAG) peptidase*. PSMA is an enzyme that is encoded by the *folate hydrolase* (FOLH1) gene in humans [53]. In the last 15 years, several radiometal-labeled PSMA inhibitors have been developed for molecular imaging and targeted therapy (Chap. 22). In 2012, the development of PSMA-HBED-CC (also known as PSMA-11 or DKFZ-PSMA-11) at the German Cancer Research Centre (GCRC) and the University Hospital at Heidelberg by Drs. Eder, Haberkorn and Afshar-Oromieh should be regarded as a major milestone in the development of radiolabeled PSMA inhibitors for molecular imaging, and targeted therapy.

PSMA-11 consists of a Glu-urea-Lys motif conjugated with the highly efficient and Ga-specific acyclic chelator HBED-CC (Fig. 12.2) via an aminohexanoic acid (Ahx) spacer [54]. The advantage of HBED-CC chelator is that it can form efficient ^{68}Ga complex at room temperature with extremely high thermodynamic stability. In the first human studies, direct comparison to [^{18}F]FCH, ^{68}Ga-PSMA-targeted PET imaging was able to detect lesions much earlier in patients with low PSA values and showed a reduced background activity in healthy tissue [55]. Subsequently, several clinical studies documented the clinical utility of ^{68}Ga-PSMA-11 (Fig. 22.23) for molecular imaging of prostate cancer [56]. The FDA approved ^{68}Ga-PSMA-11 in 2020 for PET imaging of PSMA positive prostate cancer.

12.3.3 Chemistry of Transition Metals

As shown in Table 12.6, several positron-emitting radioisotopes of transition metals such as such ^{44}Sc, ^{45}Ti, ^{52}Fe, ^{55}Co, ^{64}Cu, ^{86}Y, ^{89}Zr, and ^{94m}Tc have also been found to have suitable radioactive decay, and emission characteristics for PET imaging studies.

The definition of a transition metal according to IUPAC is "an element whose atom has a partially filled *d* sub-shell, or which can give rise to cations with an incomplete *d* sub-shell." Based on this definition, Sc and Y are not transition metals. However, it is also generally accepted that "transition metal" as any element in the d-block of the periodic table, which includes groups 3 to 12 or any element that can participate in the formation of chemical bonds with the valence electrons in two shells instead of only one. For the current discussion, the PET radiometals, ^{44}Sc and ^{86}Y, will be regarded as transition metals. The other important transition metals are ^{64}Cu, ^{89}Zr, and ^{99m}Tc.

12.3.3.1 Scandium-44

Scandium is the smallest of the rare-earth metals, with an ionic radius of 75–87 pm. Scandium readily loses 3 electrons in the outer shells (d^1s^2) and is found almost exclusively as a trivalent cation (Sc^{3+}) with the high coordination preference (CN = 6–8), and ionic bonding tendency (I_A = 10.49). It begins to hydrolyze at pH 2.5 and precipitation of $Sc(OH)_3$ occurs at pH 7–11 (Kostelnik and Orvig 2018). Sc^{3+} has a high preference for hard donating groups and favors a coordination number of eight, even in its hydrated form. DOTA is widely used for scandium-based radiopharmaceuticals. The high stability (log K_{ML} = 27.0–30.8) and pM value (23.9–26.5) support the use of DOTA analogs for the majority of Sc^{3+} based radiopharmaceuticals (IAEA-

TECDOC1945, 2021). ^{44}Sc-labeled molecular imaging probes are in pre-clinical and proof-of-concept phase clinical evaluations [57–59]. ^{44}Sc holds great promise for future applications as a novel PET nuclide for diagnostic imaging and for monitoring therapy in clinics. The relatively longer half-life (4 h) compared to ^{68}Ga provides great advantage for commercialization and distribution of doses similar to that with ^{18}F labeled radiopharmaceuticals.

12.3.3.2 Yttrium-86

Yttrium, like Sc, also loses the outer 3 electrons and is predominantly found as a trivalent cation (Y^{3+}). But the ionic radius of yttrium cation (90–108 pm) closely resembles that of lanthanides and prefers coordination number of 8 or 9 [13]. Most of Y radiotracers were developed using either DOTA or CHX-A"-DTPA for chelation. These chelates quantitatively radiolabel yttrium radionuclides at low concentrations and show kinetic stability under physiological conditions [60]. With the acyclic DTPA analogs, the stereochemistry of CHX-DTPA was shown to be of major importance, with markedly higher kinetic stability observed with CHX-A"-DTPA, compared to CHX-B″-DTPA. H_4octapa, an octa-dentate analogue of H_2dedpa based around a picolinic acid scaffold, also demonstrated high radiolabeling yields and serum stability [18].

While the potential utility of ^{86}Y-labeled peptides for PET imaging studies in patients has been documented [61], the physical half-life of ^{86}Y is suboptimal (not long enough) to follow the in vivo kinetics of labeled mAbs. It is more appropriate to use long-lived positron emitter, ^{89}Zr for developing immuno-PET to allow optimal target/background ratios with radiolabeled mAbs.

12.3.3.3 Copper-64

The relatively longer half-life and low positron energy (T½ = 12.7 h; 0.653 β^+) of ^{64}Cu is appropriate for PET imaging. Copper exhibits a rich coordination chemistry with complexes known in oxidation states ranging from 0 to +4, although the +2 (cupric) and the +1 (cuprous) oxidation states are by far the most common [62, 63]. Cu^{2+} and Cu^{+} oxidation states favor dissimilar ligand donors and coordination geometry. The electron configuration and chemical hardness of Cu^{2+} (d^9) dictates a preference for borderline hard Lewis base donors, such as aliphatic and aromatic amines, as well as carboxylate donors; however, Cu^{2+} can also accommodate softer donors, such as thiolate and carbazone [11]. Cu^{2+} can accommodate a variety of coordination numbers and geometries, including square planar, square pyramidal, trigonal bipyramidal, and octahedral. In vivo, under hypoxic conditions, Cu^{2+}, however, can be reduced to Cu^{+} oxidation state causing instability of Cu^{2+} coordination complexes. In contrast, Cu^{+} (d^{10}) exhibits a preference for soft donors (thiol, thio-ether, and imidazole) and a tetrahedral geometry.

The two well well-known ^{62}Cu-based PET imaging agents are both small metal complexes of acyclic chelator, thiosemicarbazone; ^{62}Cu-diacetyl-bis(N4-thiosemi-carbazone or ^{62}Cu-PTSM and Cu-diacetyl-bis(N4-methylthiosemicarbazone or Cu-ATSM [64]. In both cases, a Cu^{2+} center is coordinated in a square planar geometry by the two nitrogen atoms and two sulfur atoms of the thiosemicarbazone [63]. Under reducing, oxygen-deficient conditions, the reduced Cu^{+} species dissociates from the chelator and binds to intracellular proteins. This approach may provide a simple method to develop copper-based small molecule radiopharmaceuticals.

For the development of kinetically inert copper complexes, the chelators must provide a rigid coordination environment that disfavors fluxional changes of the coordination environment, and the Cu^{2+} radiolabeled complex must be resistant to reduction under physiological conditions. For several decades, most of the chelator development for Cu nuclides has focused on polyaza macrocyclic BFCs, such as DOTA, NOTA, TETA, and TE2A complexes. While DOTA complexes have shown clinical utility, the Copper complexes of TETA and TE2A exhibit greater thermodynamic stability and kinetic inertness [11]. Recently in 2020, the FDA approved ^{64}Cu-DOTATATE for PET imaging studies in patients with SSTR positive NETs. The superior quality of ^{64}Cu-Dotatate images suggest that for PET imaging studies with ^{64}Cu-labeled peptides acquired in 1–3 h after tracer administration, the DOTA chelator is able to provide adequate in vivo stability. However, to improve greater structural rigidity, cross-bridged chelators, such as

CB-TE2A, were developed. While these chelators have kinetic stability, they still require higher temperatures for quantitative labeling. The sarcophagine family of chelators (Fig. 12.4), based on hexaazamacrobicyclic cage, were also investigated to develop copper-labeled radiopharmaceuticals [65]. The Sar, DiamSar, and SarAr chelators coordinate copper extremely quickly over a pH range of 4.0–9.0 and have shown superior performance, including quantitative radiolabeling at room temperature, and excellent in vitro, and in vivo stability [66]. NOTA and NOTA type derivatives also showed fast complexation at room temperature and high kinetic inertness in vivo [67]. ^{64}Cu and ^{67}Cu (a beta emitter) is a theranostic pair which has a significant potential for the development of tracers for imaging and targeted therapy. Several ^{64}Cu-labeled PET radiopharmaceuticals are under clinical evaluation [68, 69].

^{64}Cu-DOTATATE (DetectNet)

The initial studies with ^{64}Cu-TETA-octreotide in patients with NETs showed high rate of lesion detection, sensitivity, and favorable dosimetry and pharmacokinetics [62]. Since ^{64}Cu forms more stable complex with DOTA chelator, ^{64}Cu-DOTATATE has been studied as a potential PET radiotracer for SSTR-based imaging. The first human study clearly supports the clinical use of ^{64}Cu-DOTATATE for PET studies with excellent imaging quality, reduced radiation burden, and increased lesion detection rate when compared with OctreoScan [70, 71].

In a head-to-head comparison with ^{68}Ga-DOTATOC-PET in patients with NETs, ^{64}Cu-DOTATATE-PET scans detected more lesions although patient-based sensitivity was the same for both agents [72]. Recently in a prospective trial in patients with Known or Suspected SSTR positive NETs PET/CT scan with ^{64}Cu-DOTATATE was considered a safe imaging technique that provides high-quality and accurate images at a dose of 148 MBq (4.0 mCi) for the detection of SSTR expressing NETs [73]. The lower positron energy of ^{64}Cu compared to that of ^{68}Ga (0.65 vs. 1.90 MeV), which translates to lower positron range (0.56 vs. 3.5 mm), is thought to explain the anticipated improved spatial resolution and diagnostic performance of ^{64}Cu-DOTATATE (Fig. 12.10).

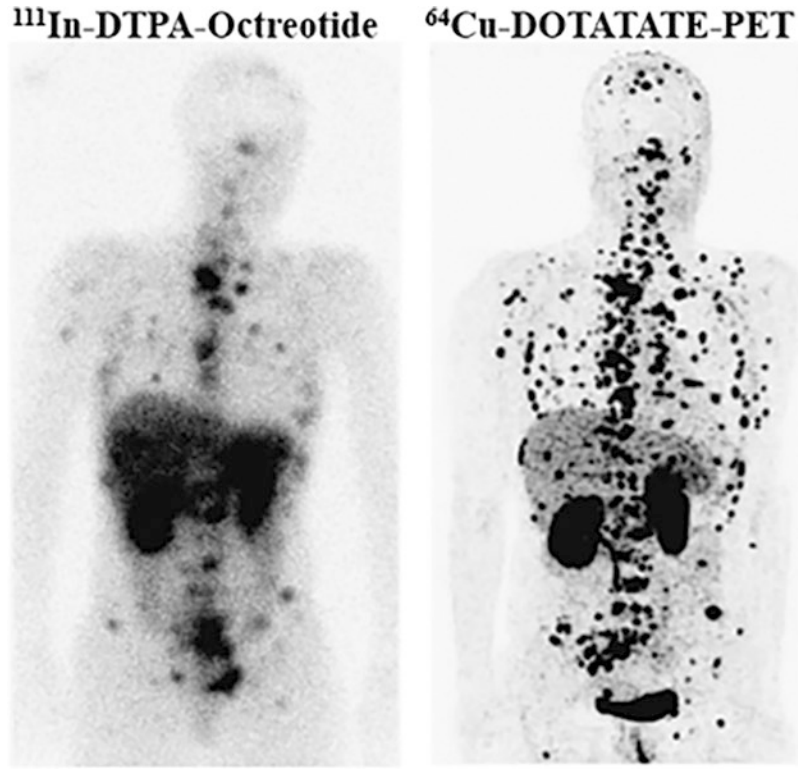

Fig. 12.10 Comparison of ^{64}Cu-DOTATE-PET and ^{111}In-DTPA-Octreotide (OctreoScan) in the same patient with NETs with multiple bone and soft tissue metastases ([71])

Additionally, the longer physical half-life of ^{64}Cu (12.7 h) may increase the shelf-life of ^{64}Cu-DOTATATE and provide a more flexible scanning window, making it attractive for routine clinical imaging.

In September 2020, the *FDA approved ^{64}Cu-DOTATATE injection (DetectNet) for the localization of SSTR-positive NETs.*

12.3.3.4 Zirconium-89

^{89}Zr, a transition metal, has an ideal physical half-life (78.4 h) and appropriate β^+ energy (E_{mean} = 0.39 MeV) for PET imaging studies [74, 75]. The most preferred method of production is based on the reaction ^{89}Y(p,n)^{89}Zr using ^{89}Y (natural abundance 100%) foil as the target material [76]. Subsequently, ^{89}Zr is purified by anion-exchange chromatography. Zr complexes with hydroxamates in acidic solutions (>1 N HCl), compared to other metallic impurities (Fe, Al, Y), that do not interact. The most common and convenient chemical form is ^{89}Zr in oxalic acid (0.5 M) with a purity >99.99% [77, 78]. The availability of carrier-free ^{89}Zr as either zirconium-89 oxalate ($[^{89}Zr(C_2O_4)_4]^{4-}$) or ^{89}Zr chloride ($[^{89}Zr]ZrCl_4$) is essential to the development of effective immuno-PET agents. ^{89}Zr is typically obtained with high radiochemical yields (~90%) and effective molar (specific) activities of around 60 GBq/μmol [79].

Zr, a second-row transition metal can exist in several oxidation states including Zr(II), Zr(III) and Zr(IV), which is its preferred oxidation state. ^{89}Zr is typically present in solution as Zr^{4+} and is a hard Lewis acid with strong affinity for hard Lewis bases such as oxygen.

When ^{89}Zr was first investigated for PET imaging, common universal metal chelators such as EDTA, DTPA, and desferrioxamine (DFO), were used to investigate the coordination requirements for ^{89}Zr complexation [80–82]. Based on these studies it was concluded that the hard oxophilic ^{89}Zr ion prefers an octadentate coordination sphere. In the ^{89}Zr–DFO complex, the three hydroxamates occupy only six of the preferred eight coordination sites of the Zr^{4+} ion (Fig. 12.11), leaving a gap in the ligand sphere where other ions and molecules can interact,

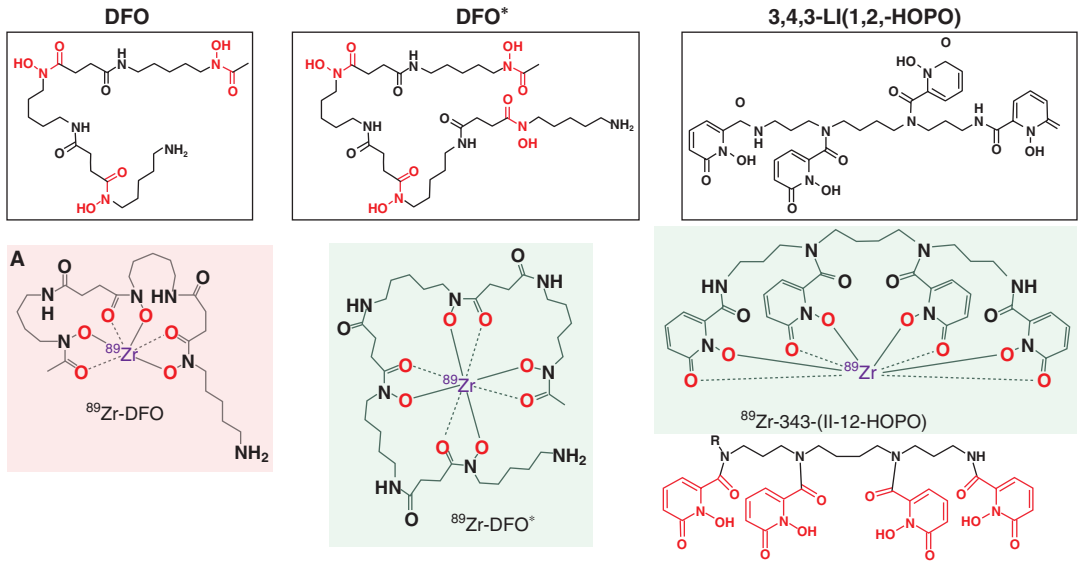

Fig. 12.11 ^{89}Zr chelating agents and the coordination complexes. DFO chelator provides six oxygen donor atoms to form hexadentate ^{89}Zr-DFO complex. In contrast, both DFO* and HOPO chelators form more stable octadentate coordination complexes

destabilize, or break the complex [83]. This has led to suboptimal stability with DFO in preclinical in vivo models and uptake of free ^{89}Zr in bones. Multiple research groups have developed octadentate chelators for ^{89}Zr to solve this issue while keeping synthesis, coupling, and radiolabeling conditions facile, and mild. A modified DFO chelator with additional hydroxamate functionalities (known as DFO*) provided the eight coordination donors for ^{89}Zr. Hydroxypyridinones (HOPOs) represent another family of compounds with good chelating properties. Recent investigations indicate that ^{89}Zr complexes of DFO* and the 3,4,3-(LI-1,2-HOPO) (Fig. 12.11) demonstrated a high inertness, qualifying them for further comparative in vivo investigation to determine the most appropriate alternative to DFO for clinical application [83–85]. In the last ten years, the potential clinical value of ^{89}Zr-based PET studies with proteins (antibodies), however, was based on the DFO chelator.

12.4 Immuno-PET and SPECT

In the early 1980s, clinical nuclear imaging studies provided the proof of principle that tumor lesions could be imaged using radiolabeled mAbs. FDA approved four radiolabeled (with ^{111}In or ^{99m}Tc) mAbs for diagnostic imaging studies. However, the diagnostic accuracy of these antibody-based scans was limited due to poor resolution of the Anger gamma cameras at that time. In addition, with the introduction of FDG-PET and PET/CT, antibody-based imaging for staging and restaging of cancer patients became obsolete. With the availability of relatively long half-life positron emitters (^{124}I, $T_{½}$ = 4.2 d and ^{89}Zr, $T_{½}$ = 3.266 d), a revival of imaging with radiolabeled antibodies based on PET imaging has taken place [86]. By combining the sensitivity of PET imaging and the specificity of antibodies, immuno-PET imaging has become a promising tool for monitoring the heterogeneity of specific gene expression, and predicting the efficacy of RIT. ^{111}In labeled mAbs are still useful for the initial development work based on SPECT imaging, however, the lack of absolute quantitation with SPECT does not support clinical utility for dosimetry studies and to monitor response to RIT.

^{89}Zr half-life is quite appropriate to study antibody biodistribution, and in the same range as the therapeutic radiometals such as ^{90}Y and ^{177}Lu. Several radiometals have been investigated for long-duration PET studies, including ^{64}Cu, ^{86}Y, and ^{66}Ga, although ^{89}Zr best fulfills many of the desired properties with its 3.27 day half-life and 23% positron emission. In addition, other favorable physical properties include minimal contamination from the 909-keV prompt γ-photons within the 511-keV PET energy window, as well as superior spatial resolution compared with many other positron-emitting isotopes as a result of the relatively low excess decay energy (E_{mean} = 396 keV).

In 2003, ^{89}Zr-labeled antibodies were introduced as chemical and biological surrogates for immunoPET studies to assess the biodistribution of ^{90}Y and ^{177}Lu-labeled antibodies [77, 78]. The first human study was published in 2006 with ^{89}Zr-labeled chimeric mAb U36 in patients with squamous head and neck cancers [87]. ^{89}Zr-PET imaging localized cervical lymph node metastasis with a high accuracy (93%). It has been shown that radiation doses of RIT with ^{90}Y-ibritumomab tiuxetan (Zevalin) can be predicted by immuno-PET with ^{89}Zr-ibritumomab tiuxetan and other ^{90}Y- and ^{177}Lu-labeled mAbs [88]. In the last 15 years, a number of studies have been conducted to investigate the feasibility of ^{89}Zr immuno-PET for predicting the efficacy of RIT and antibody therapies, imaging target expression or density, detecting target-expressing tumors, and monitoring of anti-cancer chemotherapies. Many FDA approved mAbs for immunotherapy (such as trastuzumab, bevacizumab, cetuximab, and rituximab) have been labeled with ^{89}Zr (Table 19.7) and were evaluated as radiopharmaceuticals for immunoPET [89, 90]. PET/CT scans with ^{89}Zr-trastuzumab are shown in

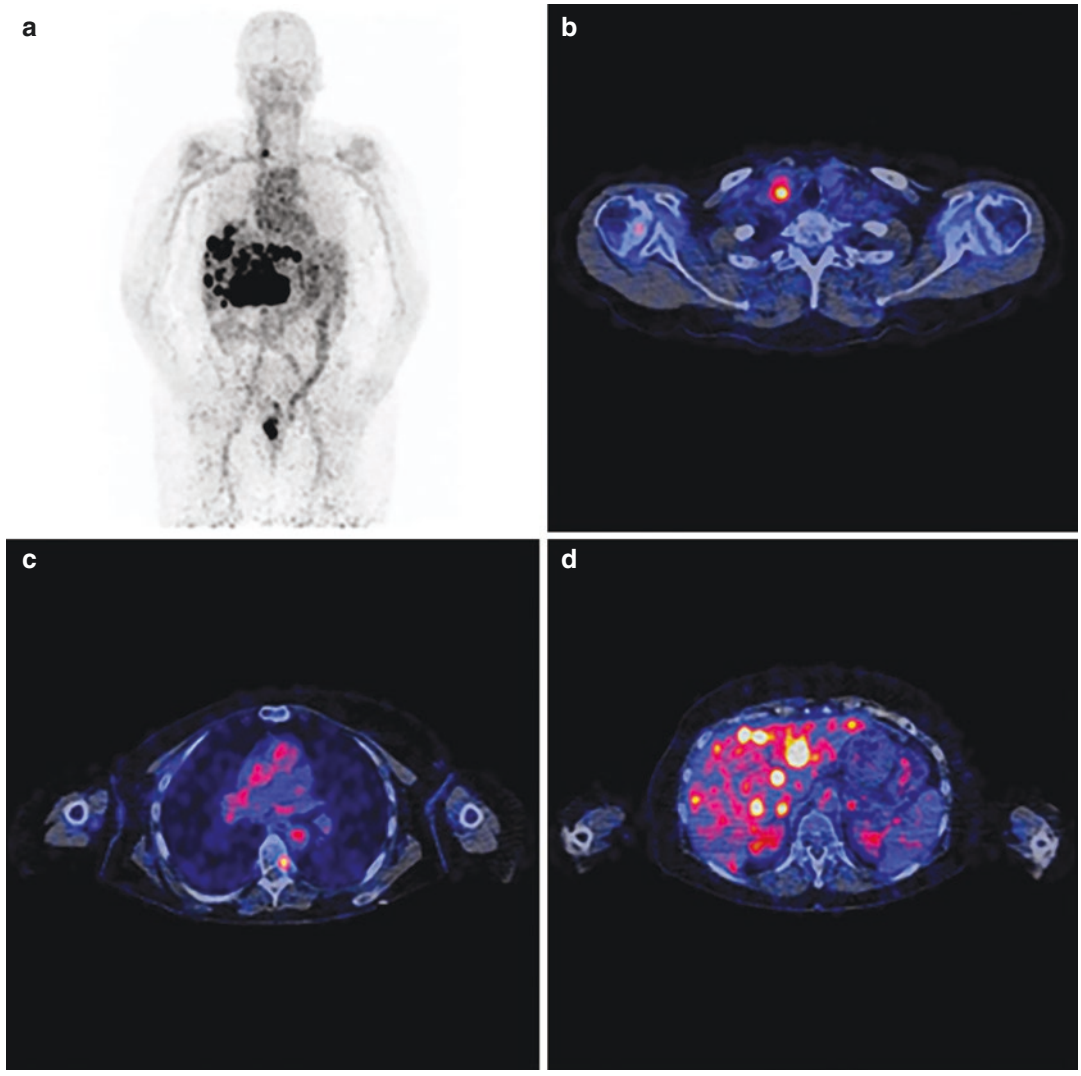

Fig. 12.12 ^{89}Zr-trastuzumab (anti-HER2 mAb)) PET/CT scan in a patient with HER2–positive metastatic breast cancer 4 days after the injection (37 MBq in 50 mg antibody). (**a**) The scan showing ^{89}Zr activity in circulation, uptake in intrahepatic metastases, and intestinal excretion. (**b**) Transverse plane of fused PET/CT of chest showing tracer uptake in cervical lymph node. (**c**) Transverse plane showing tracer uptake in metastasis (left side) in T7. (**d**) Transverse plane showing tracer uptake in liver metastases ([91])

Fig. 12.12. ^{111}In and ^{177}Lu-DOTA-huJ591 (anti-PSMA) mAb imaging studies showed excellent targeting of PSMA expression in mCRPC. However, the ^{89}Zr-IAB2M minibody (derived from J591 mAb) detected more lesions than the standatd bone scan, and FDG-PET (Fig. 12.13). Immuno-PET using ^{89}Zr has the advantages of having high resolution and high specificity but, compared to ^{18}F-labeled radiotracers, patients generally receive higher radiation dose from ^{89}Zr-mAb PET (~20–40 mSv for 37–74 MBq) [90].

12.4.1 ImmunoPET: Applications

The concept of immunoPET originally meant to describe PET imaging of radiolabeled intact full-

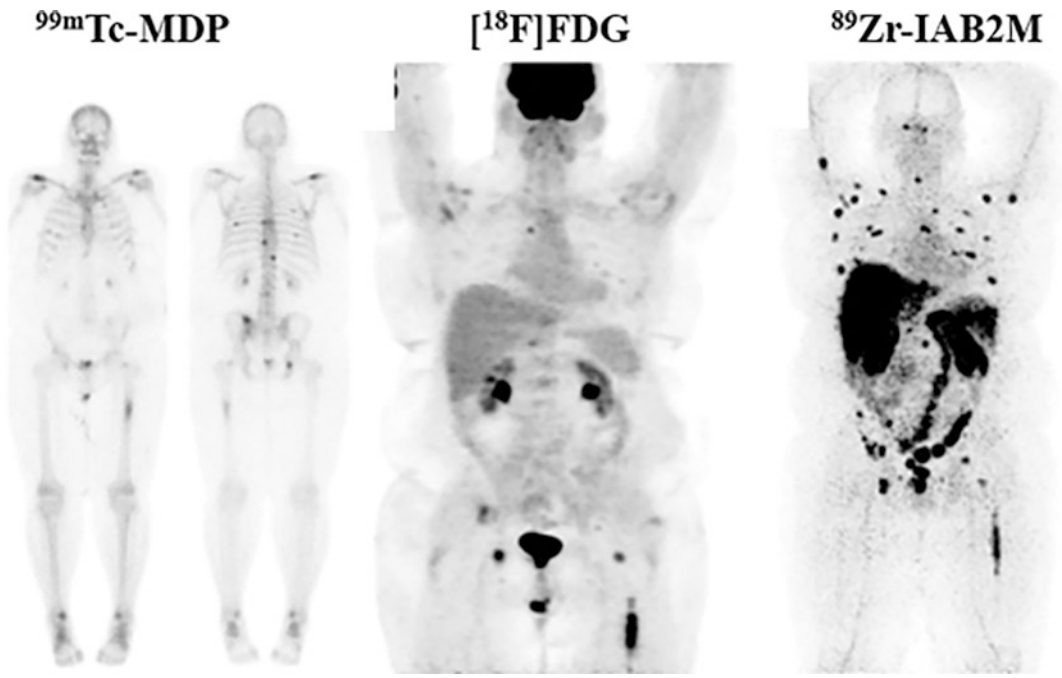

Fig. 12.13 ^{89}Zr-IAB2M-PET imaging in mCRPC. Targeting with IAB2M (minibody fragment from J591 mAb). Comparison with Bone scan and FDG-PET. ^{89}Zr-IAB2M scan shows more lesions than bone scan or FDG-PET ([92])

length mAbs. However, immunoPET now includes radiolabeled antibody fragments or mimetics as targeting vectors. A variety of radionuclides and mAbs have been used to develop molecular imaging probes for immunoPET (Table 12.9). The clinical application of immunoPET imaging has increased our understanding of tumor heterogeneity and refined clinical disease management, and includes the following applications [89]:

- To facilitate better management of cancer patients since it has the potential to provide excellent specificity and sensitivity in detecting primary tumors.
- To detect lymph node and distant metastases.
- Following immunoPET imaging, patients with positive findings can be selected for subsequent therapies (e.g., antibody therapy and antibody-based RIT), whereas patients with negative or heterogeneous findings may need multidisciplinary treatments.
- As a theranostic companion immunoPET can provide radiation dosimetry prior to administering the therapeutic radiopharmaceuticals.
- immunoPET imaging is useful for improved triage during early disease stages and to facilitate image-guided surgery.
- The information provided by immunoPET will significantly enhance the existing diagnostic methods for better tumor characterization. One can envision that, in the future, tumors may be classified not only according to their origins and mutation status but also, according to the expression of specific tumor antigens.
- Molecular imaging for cancer immunotherapy with radiolabeled probes (^{111}In and ^{89}Zr-labeled mAbs) targeting PD-1 and PD-L1 can provide in vivo, real-time, and non-invasive imaging of tumor biomarker expression, and immune responses to novel therapies.

Table 12.9 Radiolabeled mAbs and fragments as molecular imaging probes for Immuno-PET[a]

Radiolabeled antibody	Target	Targeting vector	Cancer types
^{89}Zr-Df-cetuximab	EGFR	mAb	Solid tumors
^{89}Zr-Panitumumab	EGFR	mAb	Colorectal cancer
^{89}Zr-Df-trastuzumab	HER2	mAb	Breast cancer, esophagogastric adenocarcinoma (EGA)
^{64}Cu-DOTA-trastuzumab	HER2	mAb	BC
^{89}Zr-Df-Pertuzumab	HER2	mAb	BC
^{124}I-trastuzumab	HER2	mAb	Gastric cancer, gastroesophageal cancer
^{64}Cu-DOTA-Patritumab	HER3	mAb	Solid tumors
^{89}Zr-GSK2849330	HER3	mAb	Solid tumors
^{89}Zr-lumertuzumab	HER3	mAb	Solid tumors
^{89}Zr-Df-bevacizumab	VEGF	mAb	Solid tumors
^{89}Zr-cmAb U36	CD44v6	mAb	Squamous cell carcinoma of the head and neck (HNSCC)
^{89}Zr-RG7356	CD44	mAb	Solid tumors
^{89}Zr-rituximab	CD20	mAb	Lymphoma
^{89}Zr-DFO-5B1	CA19.9	mAb	Pancreatic cancer
^{89}Zr-huJ591	PSMA	mAb	Prostate cancer
^{89}Zr-girentuximab	CAIX	mAb	Renal cell carcinoma
^{89}Zr-DFO-MSTP2109A	STEAP1	mAb	Prostate cancer
^{89}Zr-fresolimumab	TGF-β	mAb	Glioma
^{68}Ga-ABY-025	HER2	Affibody	Breast cancer
^{68}Ga-HER2-nanobody	HER2	Nanobody	Breast cancer
^{89}Zr-IAB2M	PSMA	minibody	Prostate cancer
^{68}Ga-IMP288	CEA	BsAb	Medullary thyroid cancer
^{89}Zr-AMG 211	CEA/CD3	BiTE	Gastrointestinal adenocarcinoma
^{89}Zr-Df-IAB22M2C	CD8	Minibody	Solid tumors
^{89}Zr-atezolizumab ^{111}In-atezolizumab	PD-L1	mAb	Non-small cell lung cancer (NSCLC), bladder cancer, triple negative breast cancer (TNBC)
^{89}Zr-Nivolumab	PD1	mAb	Lung cancer

[a]Table modified from [89]

The clinical studies with radiolabeled antibodies and antibody fragments are very limited but, they have, clearly, demonstrated that immuno-PET provides high resolution images needed for diagnosis and treatment assessment. More research and extensive imaging clinical trials are needed to refine immuno-PET for the diagnosis of cancers and assessment of response to therapy. ImmunoPET studies will be essential for the assessment of target antigen expression and identification of patient right patient for a specific RIT clinical trial.

12.5 Tecnetium-99m Chemistry

Technetium (Tc) was first discovered in 1937 by Emilio Segre and Carlo Perrier. Because it was artificially produced by bombarding molybdenum with deuterons, the name technetium for this new element was derived from the Greek word *technetos*, meaning artificial. Trace amounts of ^{99}Tc, however, were isolated from a uranium-rich ore in 1961 and more than 20 isotopes of technetium are known, all of which are radioactive. The most useful isotope, the metastable ^{99m}Tc ($T_{½}$ = 6.01 h), decays by isomeric transition to the relatively long-lived ^{99}Tc ($T_{½}$ = 2.1 × 10^5 year) following emission of a 140 KeV gamma photon. As previously noted, in 1958 scientists at the Brookhaven National Laboratory (BNL) reported the development of the first ^{99m}Tc generator based on the parent radioisotope ^{99}Mo. Since the 1970s, ^{99m}Tc radiopharmaceuticals have played a major role in the advancement of nuclear medicine as a diagnostic specialty. Also, since the SA ^{99m}Tc can be very high (599 Ci μmol^{-1}), it is an excellent nuclide for developing molecular imaging radiopharmaceuticals for SPECT. ^{94m}Tc, a positron-emitting radionuclide ($T_{½}$ = 53 min) with even higher theoretical SA, may also have significant potential for developing radiopharmaceuticals for use with PET.

Tc is a second row group VII transition metal that is capable of multiple oxidation sates (−1 to +7). In aqueous solution, the pertechnetate anion, $^{99m}TcO_4^?$, is the most stable chemical species with a + 7 oxidation state. Because of the similar size and charge as that of iodide (I^-), the in vivo distribution of pertechnetate is similar to that of an iodide ion [93]. However, because pertechnetate is chemically stable and inert, it cannot bind directly to any organic molecule or chelate. Following reduction by appropriate reducing agents, pertechnetate can be transformed into lower oxidation states that are chemically more reactive. Several reducing agents have been investigated with stannous chloride ($SnCl_2$) being the most widely used agent for preparing complexes of Tc(V) and Tc(I), while boron-hydrides are used to prepare organometallic Tc(I) complexes. During reduction by the stannous ion (Sn^{2+}), in an appropriate buffer and pH, the presence of a ligand stabilizes Tc in its lower oxidation state. In a specific Tc-complex, the oxidation state of Tc, however, depends on the chelate and pH [93]. As a transition metal, Tc can adopt a large number of coordination geometries, depending on the donor atoms and the type of the chelating agent. Several donor atoms, such as N, S, O, and P, geometrically arranged in a chelating molecule, can form coordination complexes with technetium. A number of ligands, such as DTPA, Dimercaptosuccinic acid (DMSA), iminodiacetic acid (IDA) derivatives (such as HIDA, DISIDA, BrIDA), phosphates, and phosphonates (such as PYP, MDP, EHDP) have been labeled with ^{99m}Tc and routinely used for diagnostic imaging studies in nuclear medicine.

The radiopharmaceutical chemistry of Tc(V) is dominated by the $[TcO]^{3+}$ core, which is stabilized by a wide range of donor atoms (N, S, O), but prefers thiolate, amido, and alkoxide ligands. Several tetra-ligand chelates designed to bind to Tc(V), typically form complexes (such as N_2S_2, N_3S, N_3O, and N_4) having square pyramidal geometries (Fig. 12.14. The ^{99m}Tc complex of mercaptoacetyltriglycine (MAG3) forms a square pyramidal complex with Tc(V) with the basal plane consisting of three nitrogen atoms and one sulfur donor atom. A variety of BFCs, such as N_2S_2 diamidedithios, N_3S triamide thiols, N_4 tetraamines or hydrazinonicotinic acid (HYNIC), have been evaluated upon conjugation to peptides to achieve labeling with ^{99m}Tc.

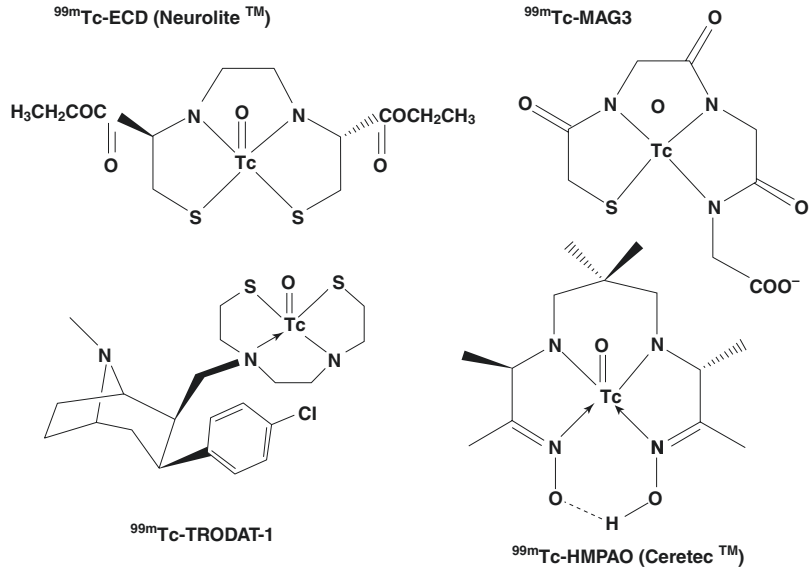

Fig. 12.14 Tc-coordination cores commonly used to develop radiometal-labeled peptides

The direct method of ^{99m}Tc labeling to peptides uses a reducing agent to break a disulfide bridge of a peptide for binding of ^{99m}Tc to thiol groups in the peptide molecules. This method often suffers from lack of specificity and poor in vivo stability. In the indirect method, ^{99m}Tc is bound to the peptide through a BFC, which can be conjugated to the peptide either before (post-labeling approach) or after labeling with ^{99m}Tc. In the 1990s several approaches have been developed to label peptides and proteins with ^{99m}Tc. New directions in developing chelators for developing ^{99m}Tc-chelate-biomolecule complex have been reviewed [11, 94]. Three important labeling methods have been developed based on three commonly used Tc-coordination environments (cores) as shown in Fig. 12.15:

- The MAG_3-based bifunctional chelates (Tc(V) oxo core).
- The *N*-oxysuccinimidylhydrazinonicotinamide system and (Tc(V) HYNIC core).
- The recently described single amino acid chelates for the Tc(I)-fac-tricabonyl core.

Mixed aminothiol-based chelators such as N_2S_2 ligand bisaminoethanethiol (BAT) and N3S ligand mercaptoacetyltriglycine (MAG_3) were developed to label biomolecules based on Tc(V) O core. ^{99m}Tc-MAG3 (Mertiatide) was developed in 1986 as an anionic kidney functional imaging agent. The parent ligand is readily derivatized as the *S*-acetyl MAG_3-ethyl ester, containing a *p*-isothiocyanatobenzyl substituent, or as the *S*-acetyl MAG3-hydroxysuccinimidyl ester for conjugation to biomolecules. In the 1990s, MAG3 ligand was used to develop ^{99m}Tc-P829 peptide (Depreotide) for somatostatin receptor imaging. The original octreotide peptide was modified to eliminate the disulfide bridge to prevent reduction during the synthesis of ^{99m}Tc-P829 complex (Fig. 12.15). Tc-MAG3 core is robust and provides chemical versatility for the development of bifunctional tracers. There are drawbacks, such as the use of stannous chloride as a reducing agent and the need for elevated pH condition, that may lead to aggregation of proteins, as well as nonquantitative radiolabeling yields [11].

An alternative pendant approach to ^{99m}Tc radiolabeling of biomolecules was provided by the introduction of hydrazinenicotinic acid (HYNIC) as a bifunctional chelator [95, 96]. HYNIC with co-ligands like tricine and ethylenediamine diacetic acid (EDDA), in the presence of $SnCl_2$ performs fast and efficient labeling. Based on this Tc(V)HYNIC core, many small molecules, pep-

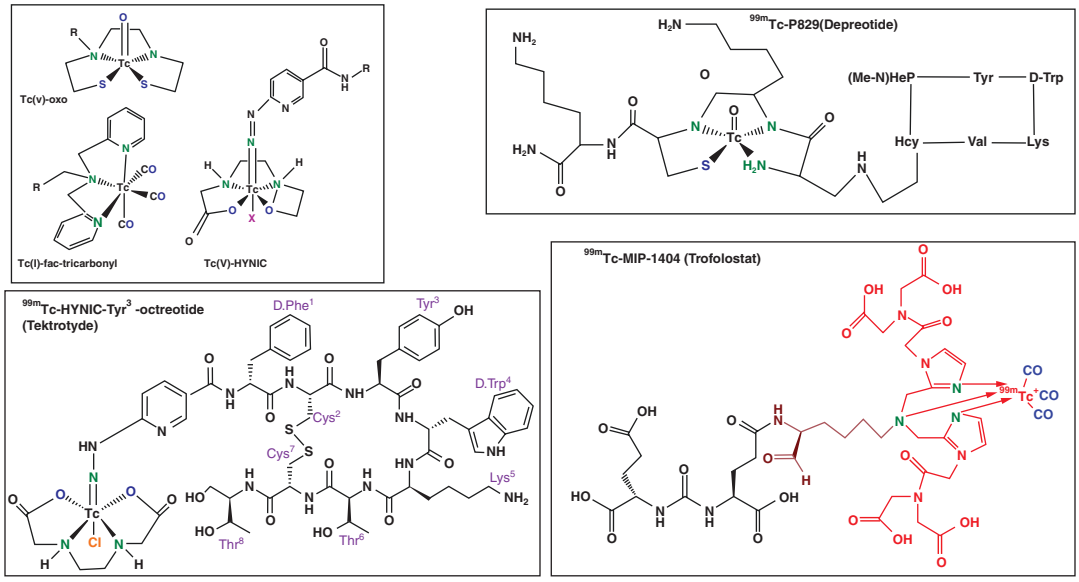

Fig. 12.15 The three important Tc-coordination cores commonly used to develop radiometal-labeled peptides. Tc-P829 was developed based on Tc(V)oxo core. Tc-HYNIC-octreotide was developed based on Tc(V) HYNIC core. Tc-MIP-1404 was developed based on (Tc(I)-fac-tricaconyl core)

tides, and proteins were labeled as imaging agents [97]. For example, Tyr^3-octreotide (TOC) was successfully labeled based on Tc-HYNIC core (Fig. 20.15). Since the HYNIC occupies only one or two coordination positions for ^{99m}Tc, co-ligands (such as tricine and EDDA) are needed to complete Tc's coordination positions. Changes in co-ligand number and type will have effect on the in vivo behavior of ^{99m}Tc radiopharmaceutical. It has been understood that [HYNIC-$^{99m}Tc(tricine)_2$] complexes usually are not very stable in solutions and could appear in different isomeric forms based on pH, temperature, and time [98].

12.5.1 Tc-Tricarbonyl Core, $[Tc(CO)_3]^+$

A major advancement in Tc chemistry has been the discovery that a highly adaptable tricabonyl Tc core makes it possible to prepare organometallic complexes in aqueous solution [99]. In an effort to develop new organometallic precursors, for the preparation of ^{99m}Tc-complexes, investigators have shown that, by treating pertechnetate $\left(TcO_4^?\right)$ with sodium borohydride ($NaBH_4$) in the presence of carbon monoxide (CO) gas, one can produce the reactive Tc(I) species, $Tc(CO)_3(OH_2)_3]^+$ [99, 100]. In this complex, the three facially oriented water molecules are sufficiently labile so that they can be readily displaced by a variety of mono-, bi- and tridentate ligands. Since it is difficult to work with CO gas, the technology is based on the use of a solid reagent, potassium boranocarbonate ($K_2H_3BCO_2$), which acts as both a reducing agent and a source of CO gas. The kit is available from Mallinckrodt (Tyco) Medical under the trade name Isolink. Further, it has been shown that both, bidentate and tridentate chelates bind rapidly to the $[Tc(CO)_3]^+$ core on a macroscopic scale and at the tracer level. ^{99m}Tc-tricarbonyl core is the favorite strategy for labeling of peptides because: a) a high labeling yield is achieved, b) purification is not needed after labeling protocol, and c) attachment of ^{99m}Tc-tricarbonyl to the peptide is easy and convenient [98]. Preclinical studies with several biomolecules labeled with Tc-tricarbonyl core revealed that these labeled compounds are biologically, kinetically, and thermodynamically stable for imaging studies.

Based on the chemistry of the organometallic fragment $[^{99m}Tc][Tc(CO)_3(H_2O)_3]+$, two radiopharmaceuticals, ^{99m}Tc-MIP-1404 and ^{99m}Tc-MIP-1405 were developed by Molecular Insight Pharmaceuticals (MIP). The preparation of these complexes was accomplished using a standard methodology and commercially available IsoLink kits (Covidien, Dublin, Ireland) and the imidazole chelator, which contains three nitrogen atoms suitable for binding to the ^{99m}Tc(I)- tricarbonyl-core (Fig. 12.15). The lead compound ^{99m}Tc-MIP-1404 (Trofolastat) completed phase III clinical trials as an imaging agent for the detection of prostate specific membrane antigen (PSMA) positive prostate cancer [101, 102].

References

1. Duclos V, Iep A, Gomez L, et al. PET molecular imaging: a holistic review of current practice and emerging perspectives for diagnosis, therapeutic evaluation and prognosis in clinical oncology. Int J Mol Sci. 2021;22:4159.
2. Weber WA, Czernin J, Anderson CJ, et al. The future of nuclear medicine, molecular imaging, and theranostics. J Nucl Med. 2020;61(12):263s–72s.
3. Halder R, Ritter T. ^{18}F-fluorination: challenge and opportunity for organic chemists. J Org Chem. 2021;86(20):13873–13884.
4. McCarthy DW, Shefer RE, Klinkowstein RE, et al. Efficient production of high specific activity ^{64}Cu using a biomedical cyclotron. Nucl Med Biol. 1997;24:35–43.
5. Williams HA, Robinson S, Julyan P, et al. A comparison of PET imaging characteristics of various copper radioisotopes. Eur J Nucl Med Mol Imaging. 2005;32:1473–80.
6. Carter LM, Kesner AL, Pratt EC. The impact of positron range on PET resolution, evaluated with phantoms and PHITS Monte Carlo simulations for conventional and non-conventional radionuclides. Mol Imaging Biol. 2020;22(1):73–84.
7. Haddad F, Ferrer L, Guertin A, et al. ARRONAX, a high-energy and high-intensity cyclotron for nuclear medicine. Eur J Nucl Med Mol Imaging. 2008;35:1377–87.
8. Robinson S, Julyan PJ, Hastings DL, et al. Performance of a block detector PET scanner in imaging non-pure positron emitters–modeling and experimental validation with 124I. Phys Med Biol. 2004;49:5505.
9. Dalen J, Visser E, Laverman P, et al. Effect of the positron range on the spatial resolution of a new generation pre-clinical PET scanner using F-18, Ga-68, Zr-89 and I-124. J Nucl Med. 2008;49:404.
10. Jødal L, Loirec CL, Champion C. Positron range in PET imaging: an alternative approach for assessing and correcting the blurring. Phys Med Biol. 2012;57:3931.
11. Boros E, Packard AB. Radioactive transition metals for imaging and therapy. Chem Rev. 2019;119(2):870–901.
12. Boros E, Holland JP. Chemical aspects of metal ion chelation in the synthesis and application antibody-based radiotracers. J Labelled Comp Radiopharm. 2018;61(9):652–71.
13. Kostelnik TI, Orvig C. Radioactive main group and rare earth metals for imaging and therapy. Chem Rev Chem Rev. 2019;119(2):902–56.
14. Meares CF, Goodwin DA. Linking radiometals to proteins with bifunctional chelating agents. J Protein Chem. 1984;3:215–28.
15. Baranyai Z, Tircsó G, Rösch F. The use of the macrocyclic chelator DOTA in radiochemical separations. Eur J Inorg Chem. 2020;2020:36–56.
16. Brunner UK, Renn O, Ki M, et al. Radiometals and their chelates. In: Wagner Jr HN, Szabo Z, Buchanan JW, editors. Principles of nuclear medicine. Philadelphia: WB Saunders; 1995.
17. Brechbiel MW. Bifunctional chelates for metal nuclides. Q J Nucl Med Mol Imaging. 2008;52(2):166–73.
18. Price EW, Orvig C. Matching chelators to radiometals for radiopharmaceuticals. Chem Soc Rev. 2014;43:260.
19. Sarko D, Eisenhut M, Haberkorn U, Mier W. Bifunctional chelators in the design and application of radiopharmaceuticals for oncological diseases. Curr Med Chem. 2012;19:2667–88.
20. Weiner RE, Thakur ML. Chemistry of gallium and indium radiopharmaceuticals. In: Welch MJ, Redvanly CS, editors. Handbook of radiopharmaceuticals. West Sussex: Wiley; 2003.
21. Green MS, Welch MJ. Gallium radiopharmaceutical chemistry. Int J Rad Appl Instrum B. 1989;16:435–48.
22. Vallabhajosula S, Harwig JF, Siemsen JK, et al. Radiogallium localization in tumors: blood binding and transport and the role of transferrin. J Nucl Med. 1980;21:650–6.
23. Kukis DL, DeNardo SJ, DeNardo GL, et al. Optimized conditions for chelation of yttrium-90-DOTA immunoconjugates. J Nucl Med. 1998;39:2105–10.
24. Srirajaskanthan R, Kayani I, Quigley AM, et al. The role of ^{68}Ga-DOTATATE PET in patients with neuroendocrine tumors and negative or equivocal findings on ^{111}In-DTPA-octreotide scintigraphy. J Nucl Med. 2010;51:875–82.
25. Al-Nahhas A, Win Z, Szyszko T, et al. What can gallium-68 PET add to receptor and molecular imaging? Eur J Nucl Med Mol Imaging. 2007;34:1897–901.

26. Dijkgraaf I, Boerman OC, Oyen WJ, et al. Development and application of peptide-based radiopharmaceuticals. Anti Cancer Agents Med Chem. 2007;7:543–51.
27. Maecke HR, Andre JP. ^{68}Ga-PET radiopharmacy: a generator-based alternative to ^{18}Fradiopharmacy. Ernst Schering Res Found Workshop. 2007;62:215–242.
28. Velikyan I. Prospective of ^{68}Ga-radiopharmaceutical development. Theranostics. 2014;4(1):47–80.
29. Pandey MK, Byrne JF, Schlasner KN, et al. Cyclotron production of ^{68}Ga in a liquid target: effects of solution composition and irradiation parameters. Nucl Med Biol. 2019;74-75:49–55.
30. Nelson BJB, Wilson J, Richter S, et al. Taking cyclotron ^{68}Ga production to the next level: expeditious solid target production of ^{68}Ga for preparation of radiotracers. Nucl Med Biol. 2020;80-81:24–31.
31. Kumar K. The current status of the production and supply of Gallium-68. Cancer Biother Radiopharm. 2019;35(3):3301163.
32. Yano J, Anger OH. A gallium-68 positron cow for medical use. J Nucl Med. 1964;5:484–7.
33. Loc'h C, Mazière B, Comar D. A new generator for ionic gallium-68. J Nucl Med. 1980;21:171–3.
34. Schuhmacher J, Maier-Borst W. A new ^{68}Ge/^{68}Ga radioisotope generator system for production of ^{68}Ga in dilute HCl. Int J Appl Radiat Isot. 1981;32:31–6.
35. Rosch F. Past, present and future of ^{68}Ge/^{68}Ga generators. Appl Radiat Isot. 2013;13:24–30.
36. Kumar K. The Current Status of the production and supply of gallium-68. Cancer Biother Radiopharm 2020;35(3):163–6.
37. Breeman WAP, Verbruggen AM. The ^{68}Ge/^{68}Ga generator has high potential, but when can we use ^{68}Ga-labelled tracers in clinical routine? Eur J Nucl Med Mol Imaging. 2007;34:978–81.
38. Zhernosekov KP, Filosofov DV, Baum RP, et al. Processing of generator-produced ^{68}Ga for medical application. J Nucl Med. 2007;48:1741–8.
39. Azhdarinia A, Yang DJ, Chao C, et al. Infrared-based module for the synthesis of 68Ga-labeled radiotracers. Nucl Med Biol. 2007;34(1):121–7.
40. Decristoforo C, Knopp R, von Guggenberg E, et al. A fully automated synthesis for the preparation of ^{68}Ga-labelled peptides. Nucl Med Commun. 2007;28:870–5.
41. Velikyan I, Maecke H, Langstrom B. Convenient preparation of ^{68}Ga-based PET radiopharmaceuticals at room temperature. Bioconjug Chem. 2008;19(2):569–73.
42. De Jong M, Bakker WH, Krenning EP, et al. Yttrium-90 and indium-111 labelling, receptor binding and biodistribution of [DOTA^0,D-Phe^1,Tyr^3]octreotide, a promising somatostatin analogue for radionuclide therapy. Eur J Nucl Med. 1997;24:368–71.
43. Otte A, Jermann E, Behe M, et al. DOTATOC: a powerful new tool for receptor-mediated radionuclide therapy. Eur J Nucl Med. 1997;24:792–5.
44. Reubi JC, Schär J-C, Waser B, et al. Affinity profiles for human somatostatin receptor subtypes SST1–SST5 of somatostatin radiotracers selected for scintigraphic and radiotherapeutic use. Eur J Nucl Med. 2000;27:273–82.
45. Hofmann M, Maecke H, Borner A, et al. Biokinetics and imaging with the somatostatin receptor PET radioligand ^{68}Ga-DOTATOC: preliminary data. Eur J Nucl Med. 2001;28:1751–7.
46. Koukouraki S, Strauss LG, Georgoulias V, et al. Evaluation of the pharmacokinetics of ^{68}Ga-DOTATOC in patients with metastatic neuroendocrine tumors scheduled for ^{90}Y-DOTATOC therapy. Eur J Nucl Med Mol Imaging. 2006;33:460–6.
47. Kowalski J, Henze M, Schuhmacher J, et al. Evaluation of positron emission tomography imaging using [^{68}Ga]-DOTA-DPhe1-Tyr^3-octreotide in comparison to [^{111}In]-DTPAOC SPECT. First results in patients with neuroendocrine tumors. Mol Imaging Biol. 2003;5:42–8.
48. Graham MM, Gu X, Ginader T, et al. ^{68}Ga-DOTATOC imaging of neuroendocrine tumors: a systematic review and metaanalysis. J Nucl Med. 2017;58:1452–1458.
49. Hennrich U, Benešová M. [^{68}Ga]Ga-DOTA-TOC: the first FDA-approved ^{68}Ga-radiopharmaceutical for PET imaging. Pharmaceuticals. 2020;13:38. https://doi.org/10.3390/ph13030038.
50. De Jong M, Breeman WAP, Bakker WH, et al. Comparison of ^{111}In-labeled somatostatin analogues for tumor scintigraphy and radionuclide therapy. Cancer Res. 1998;58:437–41.
51. Kwekkeboom DJ, Bakker WH, Kooji PPM, et al. [^{177}Lu-DOTA^0,Tyr^3]octreotate: comparison with [^{111}In-DTPA^o]octreotide in patients. Eur J Nucl Med. 2001;28:1319–25.
52. Poeppel TD, Binse I, Petersenn S, et al. ^{68}Ga-DOTATOC versus ^{68}Ga-DOTATATE PET/CT in functional imaging of neuroendocrine tumors. J Nucl Med. 2011;52:1864–1870.
53. O'Keefe DS, Su SL, Bacich DJ, et al. Mapping, genomic organization and promoter analysis of the human prostate-specific membrane antigen gene. Biochim Biophys Acta. 1998;1443:113–27.
54. Eder M, Schäfer M, Bauder-Wust U, et al. ^{68}Ga-complex lipophilicity and the targeting property of a urea-based PSMA inhibitor for PET imaging. Bioconjug Chem. 2012;23:688–697.
55. Afshar-Oromieh A, Haberkorn U, Eder M, et al. [^{68}Ga]Gallium labelled PSMA ligand as superior PET tracer for the diagnosis of prostate cancer: comparison with ^{18}F-FECH. Eur J Nucl Med Mol Imaging. 2012;39:1085–6.
56. Bois F, Noirot C, Dietemann S, et al. [^{68}Ga]Ga-PSMA-11 in prostate cancer: a comprehensive review. Am J Nucl Med Mol Imaging. 2020;10(6):349–74.
57. Chaple IF, Lapi SE. Production and use of the first-row transition metal PET radionuclides ^{43,44}Sc, ^{52}Mn, and ^{45}Ti. J Nucl Med. 2018;59:1655–9.

58. Müller M, Domnanich KA, Umbricht CA, van der Meulen NP. Scandium and terbium radionuclides for radiotheranostics: current state of development towards clinical application. Br J Radiol. 2018;91(1091):20180074.
59. Sinnes J-P, Bauder-Wüst U, Schäfer M, et al. ^{68}Ga, ^{44}Sc and ^{177}Lu-labeled AAZTA5 -PSMA-617: synthesis, radiolabeling, stability and cell binding compared to DOTA-PSMA-617 analogues. EJNMMI Radiopharm Chem. 2020;5:28.
60. Chakravarty R, Chakraborty S, Dash A. A systematic comparative evaluation of 90Y-labeled bifunctional chelators for their use in targeted therapy. J Labelled Comp Radiopharm 2014;57(2):65–74.
61. Lövqvist A, Humm JL, Sheikh A, et al. PET imaging of ^{86}Y-labeled anti-Lewis Y monoclonal antibodies in a nude mouse model: comparison between ^{86}Y and ^{111}In radiolabels. J Nucl Med. 2001;42:1281–7.
62. Anderson CJ, Dehdashti F, Cutler PD, et al. Copper-64-TETA-octreotide as a PET imaging agent for patients with neuroendocrine tumors. J Nucl Med. 2001;42:213–21.
63. Anderson CJ, Wadas TJ, Wong EH, et al. Cross-bridged macrocyclic chelators for stable complexation of copper radionuclides for PET imaging. Q J Nucl Med Mol Imaging. 2008;52:185–92.
64. Cowley AR, Dilworth JR, Donnelly PS, et al. Bifunctional chelators for copper radiopharmaceuticals: the synthesis of [Cu(ATSM)-amino acid] and [Cu(ATSM)-octreotide] conjugates. Dalton Trans. 2007;(2):209–17.
65. Di Bartolo NM, Sargeson AM, Donlevy TM, Smith SV. Synthesis of a new cage ligand, SarAr, and its complexation with selected transition metal ions for potential use in radio-imaging. J Chem Soc Dalton Trans. 2001;15:2303–9.
66. Dearling JLJ, Voss SD, Dunning P, et al. Imaging cancer using PET — the effect of the bifunctional chelator on the biodistribution of a ^{64}Cu-labeled antibody. Nucl Med Biol. 2011;38(1):29–38.
67. De Silva RA, Jain S, Lears KA et al. Copper-64 radiolabeling and biological evaluation of bifunctional chelators for radiopharmaceutical development. Nucl Med Biol. 2012;39(8):1099–104.
68. Gutfilen B, Souza SA, Valentini G. Copper-64: a real theranostic agent. Drug Des Devel Ther. 2018;12:3235–45.
69. Zhou Y, Li J, Xu X, et al. ^{64}Cu-based radiopharmaceuticals in molecular imaging. Technol Cancer Res Treat. 2019;18:1–10.
70. Carlsen EA, Johnbeck CB, Binderup T, et al. ^{64}Cu-DOTATATE PET/CT and prediction of overall and progression-free survival in patients with neuroendocrine neoplasms. J Nucl Med. 2020;61:1491–1497.
71. Pfeifer A, Knigge U, Mortensen J, et al. Clinical PET of neuroendocrine tumors using ^{64}Cu-DOTATATE: first-in-humans study. J Nucl Med. 2012;53:1207–15.
72. Johnbeck CB, Knigge U, Loft A, et al. Head-to-head comparison of ^{64}Cu-DOTATATE and ^{68}Ga-DOTATOC PET/CT: a prospective study of 59 patients with neuroendocrine tumors. J Nucl Med. 2017;58:451.
73. Delpassand ES, Ranganathan D, Wagh N, et al. ^{64}Cu-DOTATATE PET/CT for imaging patients with known or suspected somatostatin receptor–positive neuroendocrine tumors: results of the first U.S. prospective, reader-masked clinical trial. J Nucl Med. 2020;61:890–896.
74. Dejesus OT, Nickles RJ. Production and purification of ^{89}Zr, a potential PET antibody label. Appl Radiat Isot. 1990;41(8):789–90.
75. Kasbollah A, Eu P, Cowell S, Deb P. Review on production of 89Zr in a medical cyclotron for PET radiopharmaceuticals. J Nucl Med Technol. 2013;41(1):35–41.
76. Link JM, Krohn KA, Eary JF, et al. Zr-89 for antibody labeling and positron emission tomography. J Label Compd Radiopharm. 1986;23:1297–8.
77. Verel I, Visser GWM, Boellaard R, et al. Quantitative ^{89}Zr immuno-PET for in vivo scouting of ^{90}Y-labeled monoclonal antibodies in xenograft-bearing nude mice. J Nucl Med. 2003b;44:1663–70.
78. Verel I, Visser GWM, Boellaard R, et al. ^{89}Zr Immuno-PET: comprehensive procedures for the production of ^{89}Zr-labeled monoclonal antibodies. J Nucl Med. 2003;44:1271–1281.
79. Holland JP, Sheh Y, Lewis JS. Standardized methods for the production of high specific-activity zirconium-89. Nucl Med Biol. 2009;36(7):729–39.
80. Meijs WE, Herscheid JDM, Haisma HJ, Pinedo HM. Evaluation of desferal as a bifunctional chelating agent for labeling antibodies with Zr-89. Int J Rad Appl Instrum A. 1992;43(12):1443–7.
81. Severin GW, Engle JW, Nickles RJ, Barnhart TE. ^{89}Zr radiochemistry for PET. Med Chem. 2011;7(5):389–394.
82. Zeglis BM, Lewis JS. The bioconjugation and radiosynthesis of ^{89}Zr-DFO-labeled antibodies. J Vis Exp. 2015;2015:e52521.
83. Damerow H, Hübner R, Judmann B, et al. Side-by-side comparison of five chelators for ^{89}Zr-labeling of biomolecules: investigation of chemical/radiochemical properties and complex stability. Cancers (Basel). 2021;13(24):6349.
84. Bhatt NB, Pandya DN, Wadas TJ. Recent advances in zirconium-89 chelator development. Molecules. 2018;23:638.
85. Feiner IVJ, Brandt M, Cowell J, et al. The race for hydroxamate-based zirconium-89 chelators. Cancers (Basel). 2021;13:4466.
86. Chomet M, van Dongen GAMS, Vugts DJ. State of the art in radiolabeling of antibodies with common and uncommon radiometals for preclinical and clinical Immuno-PET. Bioconjug Chem. 2021;32:1315–30.
87. Börjesson PKE, Jauw YWS, Boellaard R, et al. Performance of immuno-positron emission tomography with zirconium-89-labeled chimeric monoclonal antibody U36 in the detection of lymph node

metastases in head and neck cancer patients. Clin Cancer Res. 2006;12:2133–40.
88. Perk LR, Visser GW, Vosjan MJ, et al. (89)Zr as a PET surrogate radioisotope for scouting biodistribution of the therapeutic radiometals (90)Y and (177)Lu in tumor-bearing nude mice after coupling to the internalizing antibody cetuximab. J Nucl Med. 2005;46:1898–906.
89. Wei W, Rosenkrans CT, Liu J. ImmunoPET: concept, design, and applications. Chem Rev. 2020;120(8):3787–851.
90. Yoon J-K, Park B-N, Ryu E-K, et al. Current perspectives on ^{89}Zr-PET imaging. Int J Mol Sci. 2020;21(12):4309.
91. Moek KL, Giesen D, Kok IC. Theranostics using antibodies and antibody-related therapeutics. J Nucl Med. 2017;58:83S–90S.
92. Pandit-Taskar N, O'Donoghue JA, Ruan S, et al. First-in-human imaging with ^{89}Zr-Df-IAB2M anti-PSMA minibody in patients with metastatic prostate cancer: pharmacokinetics, biodistribution, dosimetry, and lesion uptake. J Nucl Med. 2016;57(12):1858–64.
93. Deutsch E, Libson K, Jurisson S, et al. Technetium chemistry and technetium radiopharmaceuticals. Prog Inorg Chem. 1983;30:75–139.
94. Boschi A, Uccelli L, Martini P. A picture of modern Tc-99m radiopharmaceuticals: production, chemistry, and applications in molecular imaging. Appl Sci. 2019;9:2526. https://doi.org/10.3390/app9122526.
95. Babich JW, Fischman AJ. Effect of "co-ligand" on the biodistribution of ^{99m}Tc-labeled hydrazino nicotinic acid derivatized chemotactic peptides. Nucl Med Biol. 1995;22:25–30.
96. Banerjee SR, Maresca KP, Francesconi L, et al. New directions in the coordination chemistry of ^{99m}Tc: a reflection on technetium core structures and a strategy for new chelate design. Nucl Med Biol. 2005;32:1–20.
97. Mikulová MB, Mikuš P. Advances in development of Radiometal labeled amino acid-based compounds for cancer imaging and diagnostics. Pharmaceuticals. 2021;14(2):167.
98. Piramoon M, Hosseinimehr SJ. The past, current studies and future of organometallic $^{99m}Tc(CO)_3$ labeled peptides and proteins. Curr Pharm Des. 2016;22:4854–67.
99. Alberto R, Schlibi R, Schubiger AP. First application of fac-$[^{99m}Tc(OH_2)_3(CO)_3]^+$ in bioorganometallic chemistry: design, structure, and in vitro affinity of a 5-HT1A receptor ligand labeled with ^{99m}Tc. J Am Chem Soc. 1999;121:6076–7.
100. Waibei R, Alberto R, Willude J, et al. Stable one-step technetium-99m labeling of His-tagged recombinant proteins with a novel Tc(I)-carbonyl complex. Nat Biotechnol. 1999;17:897–901.
101. Schmidkonz C, Götz TI, Atzinger A, et al. ^{99m}Tc-MIP-1404 SPECT/CT for assessment of whole-body tumor burden and treatment response in patients with biochemical recurrence of prostate cancer. Clin Nucl Med. 2020;45(8):e349-e357.
102. Vallabhajosula S, Nikolopoulou A, Babich JW. ^{99m}Tc-labeled small-molecule inhibitors of prostate-specific membrane antigen: pharmacokinetics and biodistribution studies in healthy subjects and patients with metastatic prostate cancer. J Nucl Med. 2014;55(11):1791–1798.
103. Bartolo ND, Sargeson AM, Smith SV. New ^{64}Cu PET imaging agents for personalized medicine and drug development using the hexa-aza cage, SarAr. Org Biomol Chem. 2006;4:3350–7.
104. Brandt M, Cardinale J, Aulsebrook ML, et al. An overview of PET radiochemistry, part 2: radiometals. J Nucl Med. 2018;59:1500–6.
105. Chakrabarti A, Zhang K, Aruva MR, et al. KRAS mRNA expression in human pancreatic cancer xenografts imaged externally with [^{64}Cu]DO3A-peptide nucleic acid-peptide chimeras. Cancer Biol Ther. 2007;6:948–56.
106. Otte A, Mueller-Brand J, Dellas S, et al. Yttrium-90-labelled somatostatin-analogue for cancer treatment. Lancet. 1998;351:417–8.
107. Sarduy E, Ellison PA, Barnhart TE, et al. PET radiometals for antibody labeling. J Labelled Comp Radiopharm. 2018;61(9):636–51.
108. Verel I, Visser GWM, Van Dongen GAMS. The promise of immuno-PET in radioimmunotherapy. J Nucl Med. 2005;46:164S–71S.